J. Fluid Mech. (1994), *vol.* 258, *pp.* 287–316

An experimental investigation of the flow around a circular cylinder: influence of aspect ratio

By C. NORBERG

Department of Thermo- and Fluid Dynamics, Chalmers University of Technology, S-412 96, Göteborg, Sweden

(Received 21 February 1992 and in revised form 28 June 1993)

The investigation is concentrated on two important quantities – the Strouhal number and the mean base suction coefficient, both measured at the mid-span position. Reynolds numbers from about 50 to 4×10^4 were investigated. Different aspect ratios, at low blockage ratios, were achieved by varying the distance between circular end plates (end plate diameter ratios between 10 and 30). It was not possible, by using these end plates in uniform flow and at very large aspect ratios, to produce parallel shedding all over the laminar shedding regime. However, parallel shedding at around mid-span was observed throughout this regime in cases when there was a slight but symmetrical increase in the free-stream velocity towards both ends of the cylinder. At higher Re, the results at different aspect ratios were compared with those of a 'quasi-infinite cylinder' and the required aspect ratio to reach conditions independent of this parameter, within the experimental uncertainties, are given. For instance, aspect ratios as large as $L/D = 60$–70 were needed in the range $Re \approx 4 \times 10^3$–10^4. With the smallest relative end plate diameter and for aspect ratios smaller than 7, a bi-stable flow switching between regular vortex shedding and 'irregular flow' was found at intermediate Reynolds number ranges in the subcritical regime ($Re \approx 2 \times 10^3$).

1. Introduction

The crossflow around a circular cylinder has been the subject of intense scrutiny for a very long time. It is well known that the flow is dependent on, for example, Reynolds number, surface roughness, blockage and free-stream turbulence. In addition, the aspect ratio as well as the end conditions may have large influences on the flow. Probably, much of the scatter in the data reported in the literature, especially at Reynolds numbers below 10^4, is due to aspect ratio effects and/or different end conditions.

It was recognized early that different end conditions had dramatic effects in aerodynamic experiments with circular cylinders in crossflow (see e.g. Fage 1913). It was soon realized that a relatively long cylinder, with free ends exposed to the flow, was not representative of the 'infinite' cylinder, i.e. the two-dimensional case (Wieselsberger 1922). Nevertheless, effects of the diameter were sometimes found, even if the cylinders were terminated by walls or shields at low blockage ratios (see e.g. Roshko & Fiszdon 1969). The use of end plates to reduce three-dimensional effects, e.g. to shield the cylinder ends from interfering wall boundary layers, was probably initiated by Keefe (1961) and Cowdrey (1963). An optimized geometry of rectangular end plates, in the Reynolds number range from about 2×10^4 to 8×10^4, was suggested by Stansby (1974). In addition, it was assessed that a constant level of the base pressure coefficient, over the major part of the cylinder, was not a sufficient criterion for 'two-dimensional'

flow conditions. In the systematic study of both aspect ratio and blockage effects by West & Apelt (1982) the optimized end plates of the 'Stansby design' were used. At Reynolds numbers of the order 2×10^4 and at low blockages, they detected an influence from the aspect ratio up to their largest attainable value $L/D = 40$. Studies of end-plate geometry effects have also been given by Gowda (1975), Kubo, Miyazaki & Kato (1989), Stäger & Eckelmann (1991) and Szepessy (1993). In the investigation by Stäger & Eckelmann, the ratio λ/D, where λ is the distance between the leading edge of circular (or near-circular) end plates and the cylinder surface, was considered. (For circular end plates $\lambda = \frac{1}{2}(D_{EP} - D)$, where D_{EP} is the end plate diameter.) It was found that the affected region near to an end plate, in the Reynolds number range from about 300 to 5000, was smaller than or equal to five diameters (decreasing with increasing $Re/(\lambda/D)$).

The influence of aspect ratio on the critical onset Reynolds number for vortex shedding (Re_c) has been investigated by e.g. Nishioka & Sato (1974), Mathis, Provansal & Boyer (1984), Lee & Budwig (1991) and Albarède & Monkewitz (1992). The stability of the wake is greatly enhanced at aspect ratios less than about 50, resulting in a rapid increase in Re_c with decreasing L/D. At larger aspect ratios the stability seems to be more or less unaffected ($Re_c = 47 \pm 1$).

In the pioneering work of Roshko (1954), a Strouhal–Reynolds number relationship for the laminar shedding regime is presented, i.e. for Reynolds numbers from about 50 to 150. Most other investigations, however, were not able to reproduce this relationship (for a review see Williamson 1989). In Norberg (1987), however, the relationship was more or less reproduced and the dependency showed no discontinuities. In addition, an increase in the free-stream turbulence intensity from 0.1% to 1.4% did not affect the relationship. As was shown later in the work of Williamson (1988*a*, 1989), most of the discrepancies from Roshko's relation are probably due to end effects causing oblique (slanted) shedding. By converting the measured Strouhal numbers with a simple cosine factor of the shedding angle, the transformed Strouhal numbers became very close to the ones given by Roshko's relation (actually slightly lower). He also gave a recipe for production of parallel shedding: by simply tilting the end plates some degrees outward on the wake side, the shedding became parallel to the cylinder. After that other remedies with the same effect have been presented: 'end cylinders' (Eisenlohr & Eckelmann 1989); 'control cylinders' (Hammache & Gharib 1989, 1991) and 'end suction' (Williamson 1993). Interestingly, the modelling of Albarède & Monkewitz (1992), by using empirical inputs to a Ginzburg–Landau equation, suggests that it is an increase of the local Reynolds number towards the ends that produces a reduction in the shedding angle. They also noted that this was in accordance with the existing methods of producing parallel shedding (local increase in the approaching free-stream velocity towards the ends).

The existence of oblique and parallel shedding modes give rise to the following interesting question: why did the Strouhal number data of Roshko (1954) and later Norberg (1987) get so near to the relationship valid for parallel shedding, e.g. from the formula given by Williamson (1988*a*)? In both cases no particular attention was given to the end conditions; the cylinders (actually wires) were simply stretched between the walls of the wind tunnel (Roshko) or between two vertical plates inside the tunnel (Norberg). A common feature for both Roshko's and Norberg's data is that they had very large aspect ratios (Roshko: $L/D = 2128, 1381, 816, \ldots$; Norberg: $L/D = 1912$ and 954). By reviewing other experiments presented in this regime, it is found that most other investigations had used aspect ratios of the order 100. Thus, an important objective in the present work was to further investigate the influence of aspect ratio in

the laminar shedding regime with special emphasis on the effects of L/D when it is larger than about 100.

Before leaving this regime, some other experimental works have to be mentioned. First, the investigation by Gerich & Eckelmann (1982) who pointed out the importance of the cylinder end conditions. The aspect ratios ranged from 70 to 280 and the region which is directly affected by the walls (or end plates) was shown to be of the order 10 diameters. In the investigation by Van Atta & Gharib (1987) it was demonstrated that the Strouhal frequency could be greatly influenced (and even disappear) owing to very low amplitude cylinder vibrations (aeroelastic coupling). The aspect ratios were very large ($L/D > 2000$) and the cylinders were terminated at the wind tunnel walls. The measurements suggested that if there were absolutely no vibration the Strouhal–Reynolds number relationship would have no discontinuities. Effects of different end conditions and aspect ratios were further elucidated by König, Eisenlohr & Eckelmann (1990) and some convincing explanations for the previously observed discontinuities in the Strouhal–Reynolds number dependency were provided, see also Eisenlohr (1990) and König *et al.* (1992). For aspect ratios below $L/D \approx 300$ and with symmetrical end plate boundary conditions there is at least one discontinuity in the Strouhal–Reynolds number relationship. For aspect ratios larger than about 25, there is a single discontinuity which marks the changeover between an oblique mode of shedding – the so-called 'I-mode', and an (essentially) parallel mode – the 'P-mode' (König *et al.* 1990). The former mode produces the 'chevron' pattern (Williamson 1989) and it is found above a certain 'transition' Reynolds number Re_s (Hammache & Gharib 1991). The 'P-mode' is found from the onset of shedding up to Re_s. Interestingly, Re_s increases with aspect ratio (König *et al.* 1990). However, the increase with L/D appears to be rather slow ($L/D \approx 25 \Rightarrow Re_s = 60$ and $L/D \approx 100 \Rightarrow Re_s = 65$). Is it possible that the increase in Re_s with aspect ratio is 'unlimited'? If so, at sufficiently large aspect ratios, this discontinuity would not take place and the flow could then remain in the parallel 'P-mode' throughout the regime.

Another range where the aspect ratio and/or end conditions seem to have contaminated previous results is for Reynolds numbers from about 10^3 to 10^4. In this range the flow is very sensitive to disturbances (see e.g. Gerrard 1965). The work by Norberg (1987, 1989) suggests that the near-wake flow undergoes a transition at around $Re = 5 \times 10^3$ (4×10^3 at a turbulence intensity of 1.4%). A subdivision of the subcritical regime at this Reynolds number was proposed. The transition is probably related to a basic change in the three-dimensional evolution of Strouhal vortices (Norberg 1993). In addition, the one-sided axial correlation length has a maximum of about 15 diameters around the transition.

Much attention has been given to effects of aspect ratio/end conditions at Reynolds numbers higher than about 10^4, see e.g. West & Apelt (1982), Fox & West (1990), Szepessy & Bearman (1992) and Szepessy (1993). At these Re, the axial correlation length is smaller than about five diameters. The present investigation, however, is concentrated on Reynolds numbers lower than 10^4.

This parametric study is concentrated on two important quantities, the Strouhal number and the base suction coefficient. Previous measurements by the author as well as by others (e.g. Gerrard 1965; Roshko & Fiszdon 1969; Williamson & Roshko 1990) have shown that these two quantities are highly suitable as indicators for significant changes in the flow. They are also of importance in engineering applications, e.g. in disciplines such as wind engineering and flow-induced sound and vibration – the base suction coefficient is closely related to both mean and fluctuating pressure forces acting on the cylinder; the Strouhal number determines the dominating wake frequency.

In the Reynolds number range covered in this study (about 50 to 4×10^4), the effects of aspect ratio, at low blockage ratios, for diffcrent ratios of the end plate diameter to the cylinder diameter, have been investigated. The results are compared with those of an 'quasi-infinite cylinder', i.e. the case with flow conditions at mid-span independent of aspect ratio.

It should be stressed also that the end plate design may have significant effects on the influence of aspect ratio (see e.g. Lee & Budwig 1991; Szepessy & Bearman 1992). The purpose of this investigation has not been to find an optimized geometry of the end plates. Depending on the optimization criterion, however, such an investigation may find some guidance from the present results.

Hopefully, the present work can provide (i) guidelines for choosing large enough aspect ratio and (ii) accurate and reliable data on the influence of aspect ratio and relative end plate diameter. Moreover, the results for the 'quasi-infinite cylinder' might be valuable for comparison purposes, both experimentally and numerically. It is worth noting that most numerical computations of the flow around circular cylinders are two-dimensional. In a recent compilation by Graham (1993), a large number of numerical results have been compared with experimental data. In laminar flows the two-dimensional simulations are generally in good agreement with experiment but at higher *Re* the pressure forces are usually overpredicted. Interestingly, the three-dimensional simulations of nominally two-dimensional flow (see e.g. Tamura, Ohta & Kuwahara 1990; Kato & Ikegawa 1991; Batcho & Karniadakis 1991) seem to give much better predictions of these forces.

2. Experimental details

2.1. *Wind tunnel, cylinders and end plates*

The measurements were carried out in a low-speed closed-circuit wind tunnel (working section: height 1.25 m, width 1.80 m and length 2.90 m). To compensate for boundary-layer growth, the working section has corner fillets which are somewhat diminishing in size along the streamwise direction. The static pressure variation over 80% of the working section length was within ± 1% of the dynamic pressure. In the velocity range 2–32 m/s, the free-stream turbulence intensity was less than 0.06% (1–5000 Hz).

The cylinders were mounted horizontally with their axes perpendicular to the flow at a position half-way between the roof and the floor and 1.5 m downstream of the contraction outlet. At this position, the cylinders were stretched between two vertical and streamlined 10 mm thick aluminium plates, which were grounded to the floor and mutually stabilized above the roof. The passage of the cylinders was at the centre of the plates, which extended 160 mm in the streamwise direction (see figure 1).

The diameters of the cylinders were 0.202, 0.499, 1.002, 2.005, 5.98 and 19.81 mm, respectively (referred to as $D = 0.2$, 0.5, 1, 2, 6 and 20 mm, see table 1). The 0.2 and 0.5 mm cylinder diameters were measured with a microscope to an accuracy of about 1 μm whereas the others were measured with precision vernier callipers (accuracy better than 5 μm). For $D \geqslant 0.5$ mm, the variation of the diameters over the lengths were within ± 0.2% of the mean value (within ± 0.5% for $D = 0.2$ mm). The spacing between the supporting plates was 1060 mm for the 0.2 mm, 0.5 mm and the 20 mm cylinder and 480 mm for the other three diameters.

In the empty working section, the spanwise flow uniformity within these regions was better than ± 0.2%. It is important to point out that the supporting plates introduce a (symmetrical) spanwise velocity variation in the actual measurement situation. Some numerical calculations of laminar flow around these plates using a Navier–Stokes code

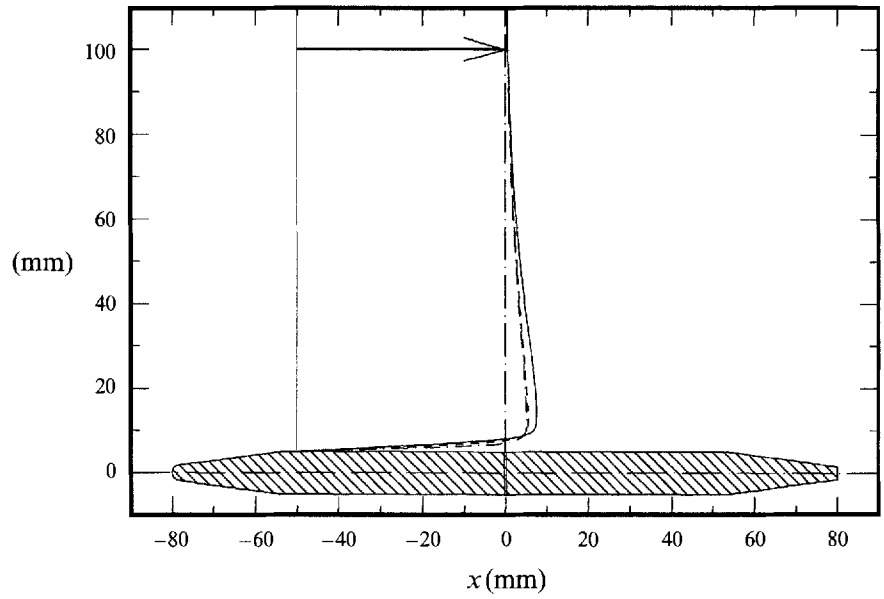

FIGURE 1. Supporting plate (shaded) with calculated (laminar) velocity profiles at the position for the passage of the cylinders (i.e. at $x = 0$). U_0(m/s): ——, 1.5; – – –, 3.0; —·—, 7.5. The length of the arrow corresponds to the undisturbed free-stream velocity, U_0.

D (mm)	$(L/D)_{NE}$ (−)	L/D (−)	D_{EP}/D (−)	D/H (%)	U_0 (m/s)	d/D (−)
0.2	—	200–5000	20	0.02	3.5, 7.5	—
0.5	—	20–2000	15, 20, 30	0.04	1.5–9.3	—
1	480	10–400	15	0.08	1.5–6.4	0.05, 0.20
2	240	5–100	10, 15	0.2	2.6–17	0.05
6	80	2–70	10, 15	0.5	3.0–26	0.065
20	53	5–50	10, 15	1.6	3.4–32	0.03

TABLE 1. Summary of parameters. $(L/D)_{NE}$ is the aspect ratio without end plates. H is the wind tunnel height and d is the pressure tapping inner diameter.

with boundary-fitted coordinates showed that there was a significant overshoot in the velocity profiles at the position for the passage of the cylinders (Davidson, private communication). At free-stream velocities 3.0 m/s and 7.5 m/s the overshoot occurred approximately 7 mm from the plates with an excess velocity of about 11% (at $U_0 = 1.5$ m/s the corresponding values were 9 mm and 15%, respectively, see figure 1). At around 80 mm and 115 mm from the plate the calculated excesses in the approaching velocity were 2% and 0.5%, respectively.

The two smallest cylinders, actually music wires, were stretched through pinholes in the supporting plates and the sidewalls and tension on the wire was produced by a rigging screw. Damping of the wires was provided by using 10 mm thick polystyrene packing foam mounted on both sides of the supporting plates and pressed against the wires from below. The other cylinders were hollow tubes, which could be rotated from the outside of the tunnel, with pressure taps at the mid-span position. By using a protractor, the frontal mean stagnation point ($\phi = 0°$) was found from the symmetry of the pressure distributions. In this way, the rearmost point ($\phi = 180°$) was found to an accuracy of about 1°.

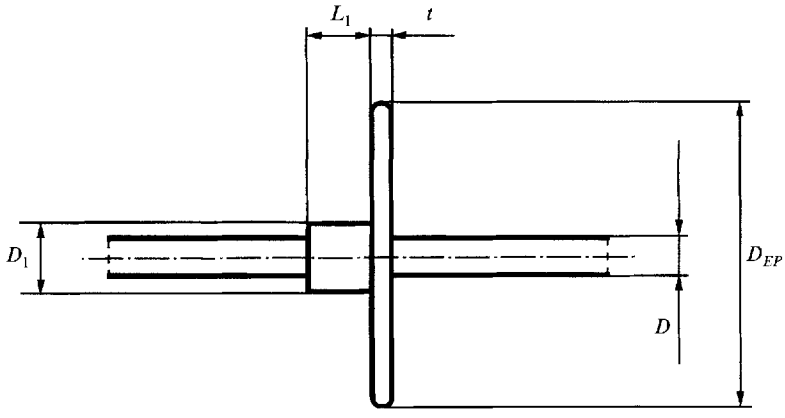

FIGURE 2. Definition sketch of the end plate geometry.

D (mm)	D_{EP}/D	t/D	D_1/D	L_1/D	Material
0.2	20	0.4	1.6	10.0	Stainless, brass
0.5	15, 20, 30	0.4	1.6	10.0	Stainless, brass
1	15	0.2	1.5	10.0	Stainless, brass
2	10, 15	0.3	1.5	1.5	Brass
6	10, 15	0.3	1.3	0.8	Plexiglas
20	10	0.1	1.5	1.1	Plexiglas
20	15	0.16	1.5	1.1	Plexiglas

TABLE 2. End-plate parameters. For definitions, see figure 2.

The maximum model blockage was 1.6% and no correction for blockage effects was applied to the data. The different aspect ratios, L/D, were achieved by varying the distance between circular end plates. Different ratios between the end plate diameter and the cylinder diameter, D_{EP}/D, were also investigated (see table 1). In the experiments without these circular end plates the supporting plates instead acted as 'end plates' (this condition is referred to as 'NE').

A sketch of the end-plate geometry is given in figure 2 and the relevant parameters are given in table 2. The thickness of the end plates (t) was smaller than 0.5 cylinder diameters throughout, whereas the diameter on the clamping side of the plates (D_1) was about 1.5 diameters. Care was taken to seal the two sides of the plates from each other. The parameters in table 2 are given for reasons of completeness. At 'small' D_{EP}/D, the most crucial parameter is probably the diameter ratio D_1/D. At first, the 2 mm cylinder was equipped with end plates having a D_1/D ratio of 2.7 ($L_1/D = 4, t/D = 0.5$). For $D_{EP}/D = 10$ and L/D lower than about 30, the measured Strouhal numbers then were significantly higher and showed a completely different behaviour when compared with the overlapping results from the 6 mm cylinder. The edges of the plates were rounded.

2.2. *Pressure measurements*

The free-stream velocity, U_0, was measured with a Pitot-static tube (United Sensor PCD-12-KL, tip diameter 4.8 mm), positioned 0.6 m upstream of the cylinders. The lowest velocity was about 1.5 m/s where this probe, according to specifications, should give out the true dynamic pressure difference. In the empty working section, the relative difference in dynamic pressure between the Pitot-static tube at this position and

another identical one at the cylinder position was within $\pm 0.5\%$. With the supporting plates there was a slight increase in the free-stream velocity between the Pitot-static tube position and the model position. The deviation between the actual approaching velocity and the measured velocity varied somewhat with the tunnel speed and was highest when the distance between the supporting plates was 480 mm (the maximum relative deviation in this case was 1.0% compared to 0.4% for the larger distance). Adjustments for this effect were applied to the data.

The base pressure coefficient is defined as:

$$C_{Pb} \equiv (P_b - P_s)/(\tfrac{1}{2}\rho U_0^2),$$

where P_b is the base pressure on the cylinder ($\phi = 180°$) and P_s is the static pressure of the free stream. The negative of this quantity, $-C_{Pb}$, will be referred to as the 'base suction coefficient' (Williamson & Roshko 1990). In the measurements, the reference static pressure was taken as the static pressure from the Pitot-static tube. In the empty working section and for velocities higher than 3 m/s, the difference in static pressure between the Pitot-static tube position and the cylinder position was less than 0.5% of the dynamic pressure (+2% at 1.5 m/s). With the cylinders having $D = 6$ and 20 mm, i.e. for Re higher than about 10^3, the measured pressure coefficients at $\phi = 0°$ were close to the expected value of unity (within 0.4%). Owing to viscous effects, at lower Reynolds numbers, there was an increase in this coefficient with decreasing Re. For instance, a value of 1.03 was measured at $Re = 200$ with the 1 mm cylinder (relative pressure hole diameter $d/D = 0.05$), in agreement with e.g. Homann (1936) and Eisenlohr (1990). Thus, it is reasonable to believe that the used reference pressure was close to the true free-stream static pressure, at least for Reynolds numbers higher than about 200 ($U_0 \geqslant 3$ m/s). The pressure differences were measured either with one micromanometer separately or in some cases with two micromanometers simultaneously. Using the former method, the dynamic pressure difference, $P_0 - P_s = \frac{1}{2}\rho U_0^2$, was measured before and after the measurement of the difference $(P_b - P_s)$. The micromanometers (Furness FC014) were individually and mutually calibrated. In addition, there was automatic correction for zero drift. The calibration indicated a linearity better than 1%. Corrections were also carried out for systematic errors arising from a difference between the normal reading where the base pressure difference was negative and the (positive) reading when the leads were switched. The voltages from the transducers were measured either with an HP Digital Voltmeter 3456A or with a digital data acquisition system (12-bit resolution). A typical value of the integration time was 60 s. At low velocities, less than about 3 m/s, with the 1 mm cylinder, integration times of the order of 10 min were necessary. At even lower velocities, e.g. less than about 1.5 m/s, the pressure signals were significantly contaminated by the throttling effect due to the small pressure hole diameter (Thom 1928). It is also possible that bias errors may arise owing to this effect since the timescales of the ambient pressure variations are of the same order as the integration times needed to obtain a statistically meaningful mean value. Thus the pressure measurements were only considered meaningful down to a Reynolds number of about 100.

In total, the overall uncertainty (at constant 20:1 odds) in the base pressure coefficient was estimated to be between $(+3\%/-5\%)$ and $\pm 1\%$ in the range from $Re = 100$ to $Re = 250$ and $\pm 1\%$ at higher Reynolds numbers. These uncertainties were also inferred from repeated experiments. The uncertainty in the free-stream velocity was estimated to be $\pm 0.4\%$ at velocities higher than 3 m/s and $\pm 0.7\%$ at lower velocities. The overall uncertainty in the Reynolds number ($Re = U_0 D/\nu$) was estimated to be $\pm 0.9\%$ for the wires and $\pm 0.5\%$ for the larger diameters.

2.3. *Strouhal frequency measurements*

The Strouhal or shedding frequency, f_S, was measured by recording the output from standard single hot wires (Dantec P15). The measurements with the music wires were carried out 10–40 diameters downstream of the cylinders. When using the larger cylinders ($D = 2$, 6 and 20 mm), the hot wire was positioned outside the separating shear layers in the near-wake region ($x/D \leqslant 5$). The shedding frequency was defined as the frequency given by the arithmetic mean of the two frequencies where the spectral level was 3 dB lower than the highest peak value in the calculated spectra. The analysing bandwidth was about 0.2% of the shedding frequency. The mean spectra were averaged on a minimum of 64 individual spectra whereas averaging a number of 100 spectra represents a more typical value. In each spectrum the fast Fourier transform (FFT) was based on 2048 samples. No data tapering was applied. The Strouhal number is defined as:

$$St \equiv f_S D/U_0.$$

A conservative estimate of the overall uncertainty in the Strouhal number was $\pm 0.8\%$ (constant 20:1 odds).

2.4. *Phase measurements*

A limited study on phase relations in the laminar vortex shedding wake was carried out with the 0.5 mm cylinder. It involved the registration of the fluctuating (sinusoidal) outputs from two hot wires (Dantec P15), one of which was fixed at a position slightly displaced from the mid-span while the other was movable to different positions on the same side as the fixed wire with respect to mid-span. Both wires were positioned at three diameters below the centre of the wake with the fixed wire 22 diameters downstream of the cylinder axis. The fixed wire served as a reference for timing. The other wire was traversed using a coordinate table; either spanwise or streamwise (downstream of the fixed wire). Photographs taken from above indicated that the angle between the spanwise traversing direction and the cylinder axis was about 0.4°. The accuracy in the movements of the second wire was better than 0.05 mm. The signals were digitized with a sampling frequency of 25 kHz corresponding to about 25 samples/period and the computed cross-correlation coefficients were based on a minimum of 128 ksamples/channel. Whenever the cross-correlation coefficient exhibited sinusoidal variations in both traversing directions an oblique shedding angle could be deduced from simple geometry. Positions for in-phase and out-of-phase conditions were also deduced from observations of 'Lissajous figures' on an oscilloscope.

2.5. *Flow visualizations*

Some smoke-wire flow visualizations were carried out in a smaller wind tunnel (working section: width 0.4 m, height 0.5 m, length 2.9 m). The free-stream turbulence intensity was less than 0.1%. The smoke-wire was made of Nichrome and the diameter was 0.05 mm. A purpose-designed electronic circuit provided the necessary electric heating pulse to the wire as well as the delayed timing pulse to the camera (Canon F1 with a 100 mm macro lens). Lighting was provided by two stroboscopes having a flash time of about 10 μs. Extremely sensitive film was used (Kodak Tmax ASA 3200).

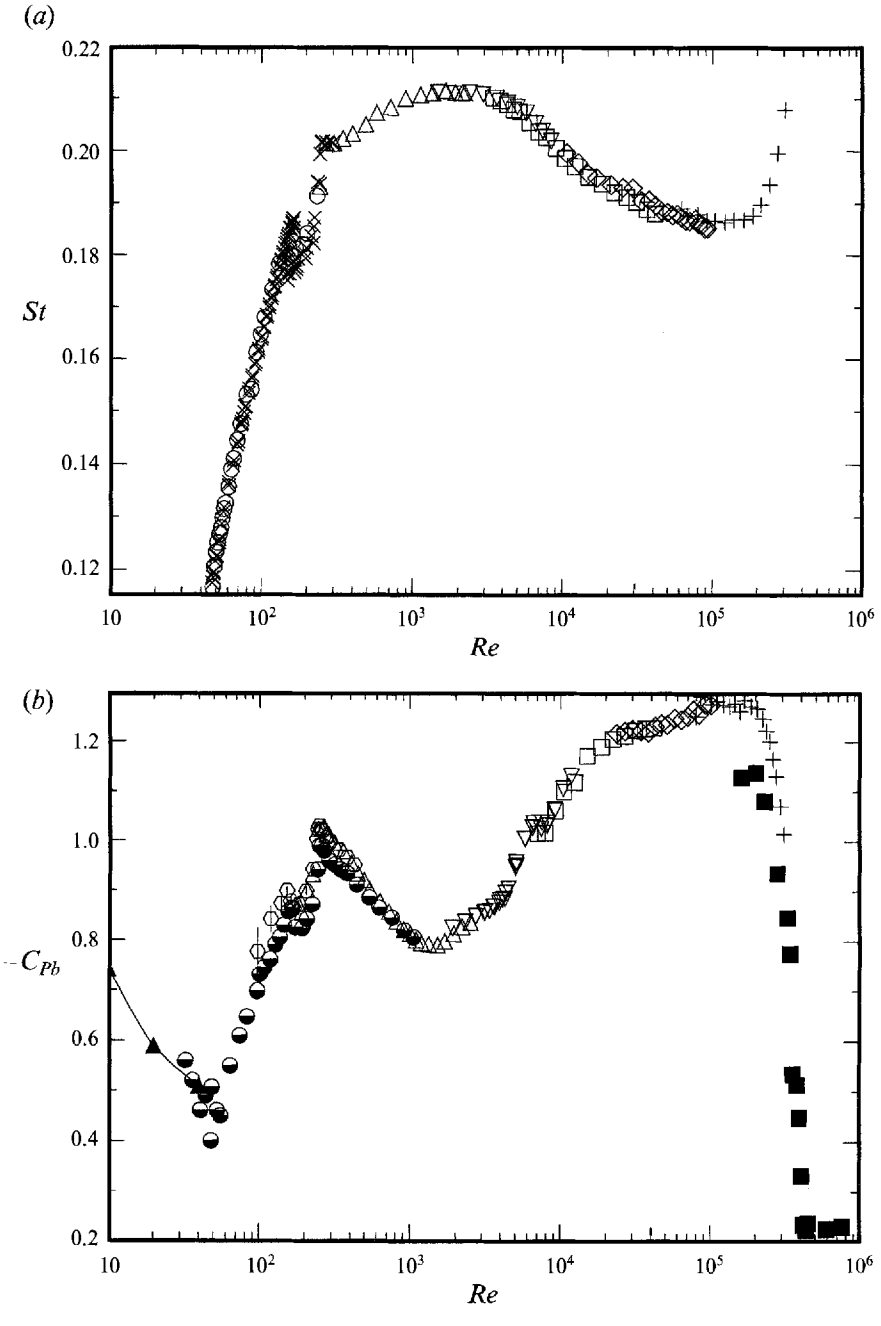

FIGURE 3. (*a*) Strouhal number and (*b*) base suction coefficient *vs.* Reynolds number. Numerical: —▲—, Dennis & Chang (1970); Experimental: ■, (D [mm], L/D) = (178, 12), Bearman (1969); ◒, (1.07, 115), Williamson & Roshko (1990); ×, (0.25, 1912); ◇, (41, 12); +, (120, 9), Norberg (1987); ○, (0.5, 2000); ○, (1, 480); △, (2, 240); ▽, (6, 80); □, (20, 53). Results for $D = 41$ mm and $D = 120$ mm are for end plates of the 'Stansby design' (Stansby 1974) and have been corrected for blockage. The vertical bars for $D = 1$ mm represent $\pm$ one standard deviation as inferred from that particular measurement.

3. Results and discussion

3.1. *Two-dimensional mean flow*

Figure 3 displays the variation of St and $-C_{Pb}$ with Re for 'large' aspect ratios. In this figure, the present data within the laminar shedding regime are supposed to be valid for parallel shedding, i.e. the mode with the highest possible frequency. A separate phase study with the 0.5 mm cylinder at $Re \approx 100$ (see §2.4 for experimental details) showed that the shedding was essentially parallel with the cylinder axis (within $\pm 1°$) up to about 100 diameters from mid-span. Farther away the shedding became progressively more slanted (away from the axis) and at around 200 diameters from mid-span the local shedding angle was about 6°. The shedding frequency was constant throughout the observed area. Moreover, the cross-correlation measurements indicated a more or less perfect correlation between the vortex filaments having the same sign of rotation (correlation coefficients higher than 0.993). The experimental set-up did not permit phase measurements across the mid-span. It can be conjectured, however, that more or less parallel shedding was present within a symmetrical central portion of the span, with a spanwise extent of about 200 diameters. As discussed further in the next section the presence of the parallel mode was not due to the large aspect ratio in these experiments ($L/D = 2000$). Instead, its appearance was due to a slight symmetrical increase in the approaching free-stream velocity towards the ends of the cylinder – an effect which came into play when the end plates were placed close to the supporting plates, see figures 1 and 6. What about the author's previous Strouhal number data (Norberg 1987) in this regime? Shedding angles were not measured at that time. However, since supporting plates of the same thickness as in the present experiments were used (although they had a slightly different nose profile and did not extend through the whole height of the working section), it can be assumed that there was a local increase in the approaching velocity towards the ends. Thus, it seems likely that parallel or very near-parallel shedding was indeed present also in that work. The characterization of these laminar cases as being representative for 'large' aspect ratios is indeed very doubtful. Whether the limiting case of 'infinite' aspect ratio will produce parallel shedding at these Reynolds numbers, irrespective of the end conditions, has yet to be proven. As shown in the next section, the present results do not indicate such a scenario. Perhaps a better characterization of the cases in figure 3 is two-dimensional mean flow, i.e. flows with an assumed negligible mean spanwise component of velocity within a substantial central region.

After the onset of shedding at $Re \approx 47$, the Strouhal number showed a continuous increase up to $Re \approx 150$, where the regular laminar shedding was occasionally disrupted by a change to three-dimensional flow. Beyond $Re \approx 168$ no regular laminar shedding could be established. As already noted by Williamson (1988*b*), this so-called '1st transition' towards turbulence is associated with a hysteretic discontinuity in the Strouhal–Reynolds number relationship, see also figure 4(*b*). In figure 4(*a*), the present Strouhal numbers which are supposed to be essentially for parallel shedding can be compared with the relations given by Roshko (1954) and Williamson (1988*a*). When taking the present overall experimental uncertainty into account, the agreement with Williamson's relation is excellent. This relation was found by fitting a quadratic to the data for the Roshko number $Ro = St\,Re$ as a function of the Reynolds number Re, i.e.

$$St = A/Re + B + C\,Re.$$

The parallel shedding data of Williamson gave the following constants:

$$A = -3.3265, \quad B = 0.1816, \quad C = 1.600 \times 10^{-4},$$

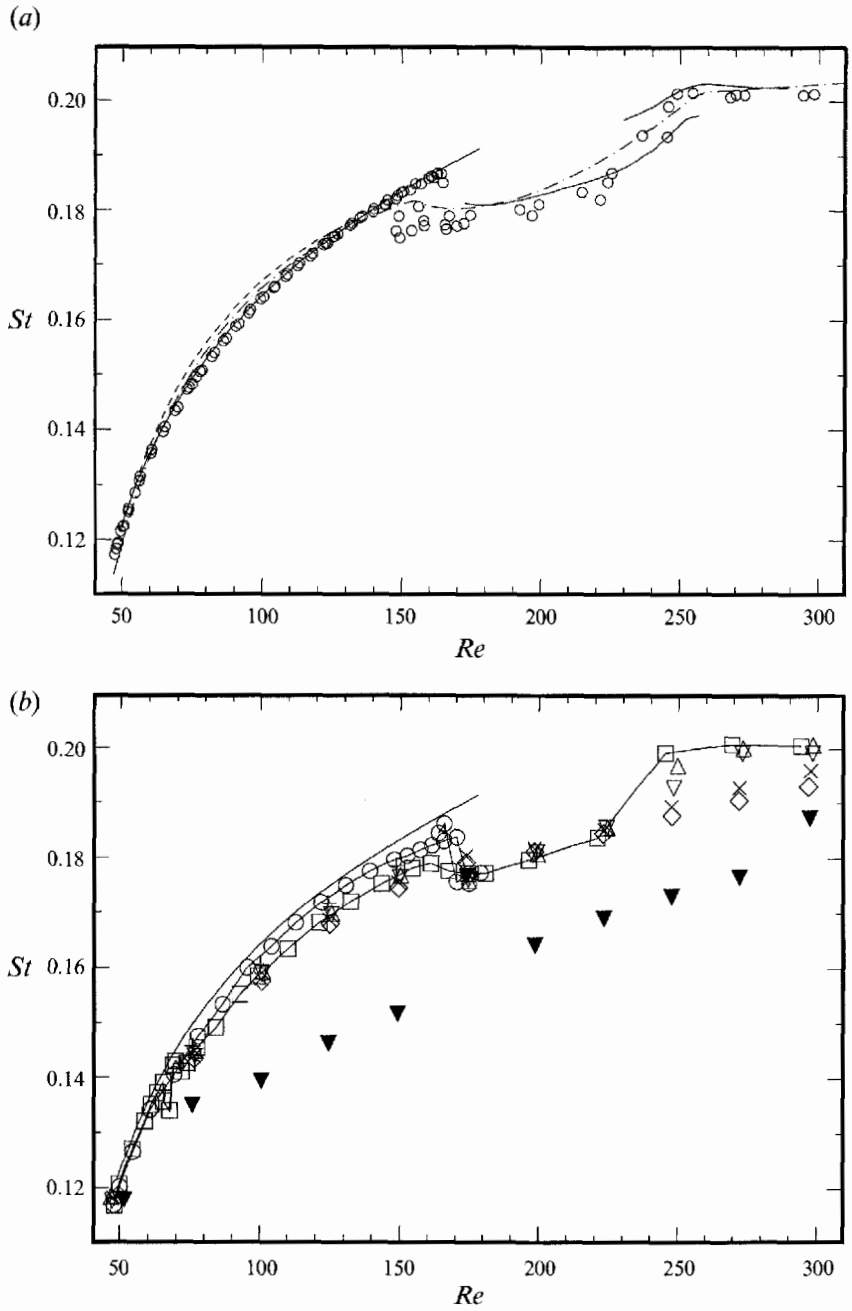

FIGURE 4. Strouhal *vs.* Reynolds number at low *Re*. (*a*) Comparison with previous data. (*b*) Present data for $D = 0.5$ mm. (*a*) ——, Williamson (1988*a*, *b*). The line in the laminar shedding regime represents the parallel shedding formula from Williamson (1988*a*); – – –, $St = 0.212(1-21.2/Re)$, Roshko (1954); —·—, Norberg (1987); ○, $L/D = 2000$, $D_{EP}/D = 20, 30$. (*b*) –○–, $(L/D, D_{EP}/D) = (1750, 30)$; +, (1500, 20); –□–, (1000, 15); △, (200, 20); ▽, (100, 20); ×, (40, 20); ◇, (30, 30); ▼, (20, 20).

with an average percentage deviation of 0.06%. On average, the percentage deviation between the present data and Williamson's relation was −0.3%. A least-square fit to the present data up to $Re \approx 165$, including only those points above $Re \approx 150$ where the shedding was regular, gave the following constants:

$$A = -3.458, \quad B = 0.1835, \quad C = 1.51 \times 10^{-4},$$

with an average deviation of 0.15% (71 points).

No discontinuities could be traced in the present *St*–*Re* relationships at $L/D = 2000$ ($D = 0.5$ mm). During the phase study, the variation of shedding frequency with velocity for the case ($L/D = 2000, D_{EP}/D = 20$) was repeated (the measurement accuracy for both velocity and frequency was further improved during these experiments). Once again the variation was continuous. Moreover, from a Reynolds number slightly above the onset and up to about $Re = 150$, the phase between a point close to mid-span and a point 100 diameters away from there in the axial direction remained more or less constant. As indicated earlier, the shedding pattern in between these points at $Re \approx 100$ was essentially parallel. This implies that there was no fundamental change in the shedding pattern within this range of Reynolds numbers. Thus the assumption of parallel shedding seems justified.

Also, at low Reynolds numbers, it should be noted that there is a slight difference in the level of the base suction coefficient between the present data and the data of Williamson & Roshko (1990). In a personal communication, Williamson considered possible reasons for such a difference (e.g. the pressure hole diameter). Despite an intensive and much stimulating exchange of ideas and information no definite conclusion about this matter could be drawn (see Williamson & Roshko 1990). However, the minor increase of the free-stream velocity owing to the supporting plates was not considered at that stage. The adjustments for this effect brought the data closer to the data of Williamson & Roshko (1990). In addition, at the lowest velocities (less than about 3 m/s) there was a small but positive difference between the used static pressure and the static pressure at the cylinder position in the empty working section (§2.2). At the lowest Reynolds number for the 1 mm cylinder ($U_0 = 1.5$ m/s $\Rightarrow Re \approx 100$) this difference indicated a possible reduction of about 2% in the measured base suction coefficient. However, for all other cylinders the lowest velocity was higher than 3 m/s where this effect was considered negligible.

The variation in Strouhal number and base suction coefficient with Reynolds number was mutually connected with a major break point at $Re \approx 250$, where the base suction coefficient peaked at a value of about 1.03, see e.g. figures 3(*b*), 4(*a*) and 7 (this peak value showed a small increase with decreasing relative hole diameter). The present investigation also found evidence supporting the finding by Williamson (1988*b*) that the measured spectra in the upper end of the transition regime actually exhibit two adjacent fundamental peaks (Williamson, personal communication). The spectra within this regime were, however, quite broadbanded. By using the present definition of the Strouhal frequency, as described in §2.3, only one single peak frequency was considered.

At Reynolds numbers in the subcritical regime (approximately $250 < Re < 2 \times 10^5$), the variations of *St* and $-C_{Pb}$ with *Re* were such that a decrease in Strouhal number was associated with an increase in base suction coefficient (and *vice versa*). In this regime the transition to turbulence occurs before the vortices roll up (Bloor 1964). At *Re* lower than 250, however, where the vortex formation is laminar, the interrelation changed, i.e. an increase in *St* was associated with an increase in the base suction.

Both $-C_{Pb}$ and *St* had a local maximum at the end of the laminar shedding regime

($Re \approx 160$), respectively. At $Re \approx 1500$, there was a local minimum in base suction coefficient ($-C_{Pb} = 0.78$) and a maximum in Strouhal number ($St = 0.211$–0.212). In addition, the mean pressure drag coefficient and the r.m.s. lift coefficient reach local minimum values at this Re (Norberg 1993). It should also be mentioned that there is a close resemblance between the variations in the so-called vortex formation length and the base pressure coefficient (see e.g. Norberg 1987). For instance, a local maximum in the vortex formation length occurs at $Re \approx 1500$. At around $Re = 5 \times 10^3$, both St and $-C_{Pb}$ showed a significant variation with Reynolds number. The shedding frequency at Reynolds numbers lower than this value, except within the transition regime (approximately $160 < Re < 250$), is extremely narrow-banded whereas at higher Reynolds numbers in the (upper) subcritical regime, the shedding frequency is time-dependent and has a significantly higher relative bandwidth (see e.g. Blevins 1985; Norberg 1989, 1993). The increase in base suction with increasing Re was followed by a plateau at around $Re = 7 \times 10^3 (-C_{Pb} = 1.02)$ and then gradually increased to reach a maximum at around $Re = 2 \times 10^5 (-C_{Pb} = 1.28)$ where it dropped when entering the critical regime. The plateau at $Re \approx 7 \times 10^3$ did not become visible until the aspect ratio was larger than about 50, see figure 9. The Strouhal number passed through the value of 0.2 at around $Re = 10^4$ and decreased to the value of 0.187 before increasing when entering the critical regime. It can be concluded from figure 3 that the Reynolds number was important throughout the whole range. The variations in Strouhal number and base suction coefficient were within the following limits in the Reynolds number range from about $Re = 250$ to 3×10^5: $St = 0.199 \pm 0.013$, $-C_{Pb} = 1.03 \pm 0.25$ (relative variations of $\pm 6.5\%$ and $\pm 24\%$, respectively).

3.2. *Reynolds numbers lower than about* 250

Within the experimental uncertainty, and for aspect ratios larger than about 40, the Reynolds number where the onset of laminar vortex shedding occurred (Re_c) was independent of both aspect ratio and relative end plate diameter ($D = 0.2$ mm: $L/D \geqslant 2000$; $D = 0.5$ mm: $L/D \geqslant 50 \Rightarrow Re_c = 47.4 \pm 0.5$). The associated critical Roshko number was $Ro_c = 5.50 \pm 0.07$. At smaller aspect ratios the onset was delayed; $L/D = 30 \Rightarrow Re_c \approx 49.5$ and $L/D = 20 \Rightarrow Re_c \approx 51.5$. The semi-empirical model of Albarède & Monkewitz (1992) suggests the following relation for Re_c, as a function of the aspect ratio:

$$Re_c = Re_{c0} + C(L/D)^{-2}.$$

Their own measurements as well as others (see e.g. Nishioka & Sato 1974; Mathis *et al.* 1984; Lee & Budwig 1991), suggest that $Re_{c0} = 47.0$–48.4 and $C = (1.6 \pm 0.5) \times 10^3$. The present critical Reynolds numbers fit well into this relation ($Re_{c0} = 47.4$, $C \approx 1.8 \times 10^3$). No hysteresis behaviour was observed.

The frequency measurements with the 0.5 mm cylinder, see figure 4(*b*), indicated that the Strouhal numbers were more or less independent of the aspect ratio in the range from about $L/D = 40$ to $L/D = 1000$. For all these aspect ratios a discontinuity in the Strouhal–Reynolds number relationship was indicated (at a Reynolds number somewhere between 60 and 70). As shown by e.g. Williamson (1989) and König *et al.* (1990), this type of discontinuity is caused by a transition between two modes of vortex shedding. A discussion about the different frequency cells which occur at Reynolds numbers around this transition can be found in König *et al.* (1990). The following description applies for cylinders bounded by end plates in uniform flow and at aspect ratios larger than about 30. From the onset of shedding up to $Re \approx 55$ there is a single cell with a constant shedding frequency. As the approaching velocity decreases very close to the end plates the shedding becomes curved and eventually the shedding

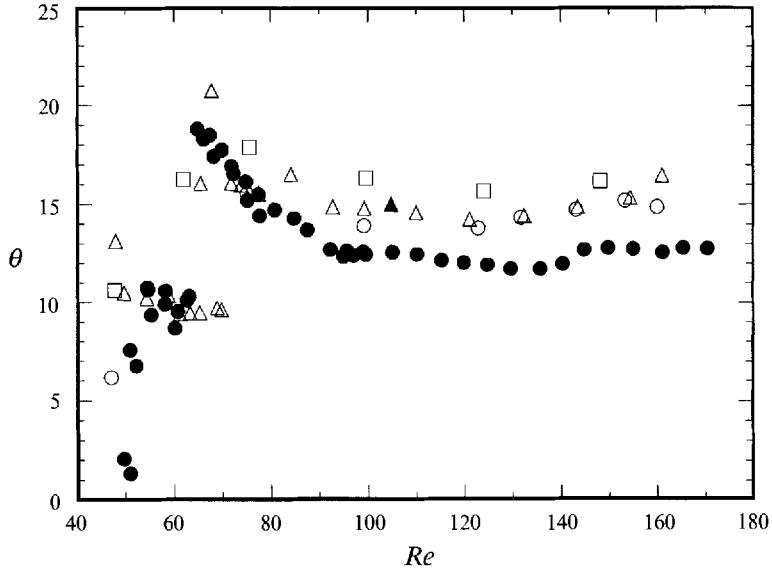

FIGURE 5. Shedding angles *vs.* *Re*: (△, ▲), $L/D = 1000$; ○, $L/D = 100$; □, $L/D = 50$; ●, $L/D = 90$, Williamson (1989). Open symbols: calculated from Williamson's formula; filled symbols: measured.

disappears (presumably when the local *Re* reaches the onset value). Outside this region the shedding is parallel. End cells with a lower frequency associated with slanted shedding develop at $Re \approx 55$. However, at Reynolds numbers below the discontinuity there is still a central spanwise region in which the shedding is essentially parallel. This is the 'P-mode'. On each side of this 'cell' there is an intermediate oblique mode with a slightly lower frequency – the 'I-mode'. The mismatch in shedding frequency forces the vortex filaments on each side to join together by 'vortex splitting' and this occurs within a narrow region – the 'IP-node'. The frequency in the end cells is even lower than in the intermediate mode and correspondingly the shedding angle is higher. The 'EI-node' between this 'E-mode' and the intermediate mode occurs at around ten diameters from the end plate. Starting off at a Reynolds number of about 60 the IP-node moves rapidly away from the end plates with increasing *Re*. The transition occurs when the distance between the two IP-nodes is less than some critical minimum distance and at Reynolds numbers above the discontinuity the P-mode is absent; instead the central region is occupied by the I-mode. As this mode involves a more or less constant shedding angle the result with perfectly symmetrical conditions will be a wedge-type 'chevron' shedding pattern (Williamson 1989).

A typical discontinuity behaviour for the shedding frequency at mid-span can be seen in figure 4(*b*) where the data points for $L/D = 1000$, $D_{EP}/D = 15$ are joined with a line. At Reynolds numbers lower than 65 the Strouhal numbers followed the upper limit associated with parallel shedding ($L/D = 2000$, see previous section). A discontinuity then appeared at $Re \approx 68$ and for *Re* higher than about 72 the data points were 3–7% below those given by $L/D = 2000$. Thus the 'transition' Reynolds number in this case was $Re_s \approx 70$. At larger aspect ratios with the 0.5 mm cylinder ($L/D \geqslant 1500$) and for Reynolds numbers higher than about 70 the Strouhal numbers gradually approached the parallel shedding curve of Williamson (1989). When parallel shedding was reached there was no discontinuity. Why did the Strouhal numbers exhibit this delayed increase targeting towards the parallel shedding value? As

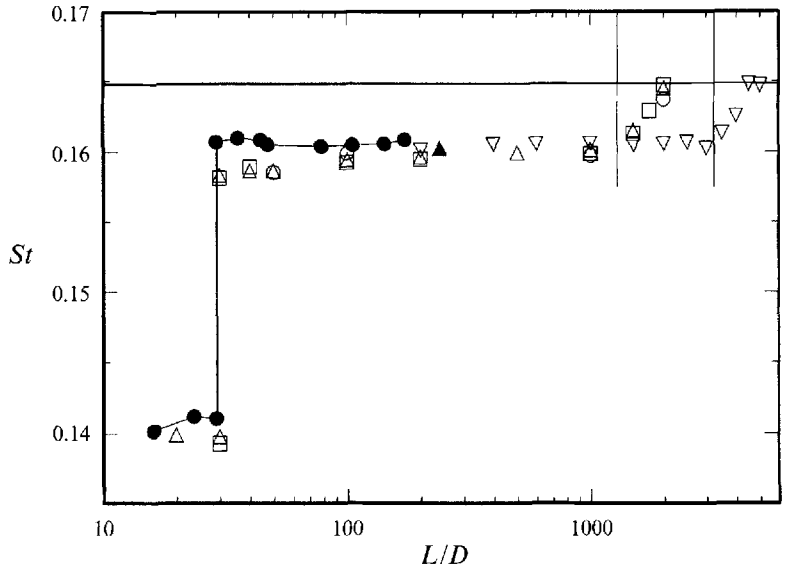

FIGURE 6. Strouhal number *vs.* aspect ratio at $Re = 101$. The vertical lines correspond to positions where the end plates were 205 mm from the supporting plates ($D = 0.5$ mm: $L/D \approx 1300$; $D = 0.2$ mm: $L/D \approx 3250$). The increase in Strouhal number with increasing L/D beyond these approximate limits is due to an associated increase in the approaching velocity at around the end plates. The horizontal line corresponds to the parallel shedding value as calculated from Williamson's formula ($St = 0.1648$). Williamson (1989): —●—, $D_{EP}/D = 12.2$; ▲, $D_{EP}/D = 25$; Present data: ○, (D [mm], D_{EP}/D) = (0.5, 15); △, (0.5, 20); ▽, (0.2, 20); □, (0.5, 30).

premised in the previous section the answer is to be found from a change in the boundary conditions. We will return to this topic later on in this section (figure 6).

By using Williamson's formula (1988*a*) the expected shedding angle can be calculated from the present data, i.e. as:

$$\theta = \cos^{-1}(St/St_{\parallel})$$

where $St_{\parallel}$ is the Strouhal number from the formula. As seen from figure 5, the expected angles from the present data at aspect ratios between 50 and 1000 ($D = 0.5$ mm) compare favourably with the observed angles as given by Williamson (1989*a*). It should be noted that the slight difference in level, of the order of 2°, as compared with Williamson's data at Re higher than about 80, actually represents a deviation in the Strouhal number less than 0.8%. Some part of this deviation might be due to different end plate geometries. The phase measurements carried out at $Re = 105$ and for ($L/D = 1000$, $D_{EP}/D = 15$) showed that the oblique angle of shedding in this case was $\theta = 14.8°$ with a streamwise (wake) wavelength of 5.3 diameters. Following Williamson (1989*a*), a multiplication of this oblique-shedding wavelength with $\cos\theta$ corresponds to the parallel-shedding wavelength. Using this transformation the wavelength becomes 5.1 diameters – in agreement with the parallel shedding data of Williamson (1989*a*). As also shown in figure 5 the measured angle of shedding at $Re = 105$ is in excellent agreement with the expected angle from the Strouhal number data.

The effects of aspect ratio and relative end plate diameter at a Reynolds number of 101 are depicted in figure 6. The horizontal line represents the Strouhal number as given by Williamson's relation for parallel shedding at this Reynolds number. The data of Williamson (1989), which are for $L/D \leqslant 250$, compare fairly well with the present data (maximum deviation of about 2%). The most astonishing feature from the

present results is the apparent strong influence of the diameter at aspect ratios larger than about 1000 (the end plates were geometrically similar to each other, see table 2). For the 0.5 mm cylinder the Strouhal number was practically constant between $L/D = 100$ and $L/D = 1000$. At larger aspect ratios ($L/D \geqslant 1500$) there was an increase in St and at $L/D = 2000$ the 'parallel value' was reached. Within the experimental uncertainty, the Strouhal numbers at the plateau ($St = 0.16$) were independent of the relative end plate diameter. For the 0.2 mm cylinder the increase towards the parallel value was delayed until an aspect ratio somewhere between 3000 and 3500 was reached. The crucial point is that the departure from the plateau-level, for each diameter, occurred when the end plates were at around the same distance from the supporting plate. When using estimated 'critical' aspect ratios of 1300 and 3250 ($D = 0.5$ mm and 0.2 mm) the distance comes out as being approximately 205 mm from the plates. At this position the excess in the free-stream velocity was calculated to be as low as 0.2%. However, at the maximum aspect ratios for each diameter ($L/D = 2000$ for $D = 0.5$ mm and $L/D = 5000$ for $D = 0.2$ mm) where the distance is only 30 mm the velocity excess was calculated to be 7.5%, see figure 1. It is interesting to note that also the case ($D = 0.2$ mm, $L/D = 4500$) reached the 'parallel value'. At this distance from the supporting plates the calculated velocity excess was 2%. Evidently, a symmetrical increase in the free-stream velocity towards the ends can induce parallel shedding at $Re > Re_s \approx 70$. To be fully effective, however, the excess in the approaching velocity at around the end plates has to reach some critical value – which in the present case evidently was of the order 2%. The situation has a close resemblance with the 'end suction' method suggested by Williamson (1993). In this method (of manipulating with the shedding pattern) suction is applied locally at some distance downstream of the cylinder axis and parallel shedding can be induced when an equal amount of suction above some threshold is applied at two spanwise positions. The corresponding velocity increase associated with this threshold suction is also of the order 2% (Miller & Williamson 1993). In fact, all methods which have been suggested for producing parallel shedding in the laminar shedding regime seem to work on the principle that there should be a local increase in the velocity at the ends. As the formation of cells with oblique shedding is caused by the restraint imposed from the unavoidable velocity decrease towards the end plates, it is understandable that this restraint can be reduced in cases where the effect is locally compensated for, i.e. by an increase in the approaching velocity. At the optimum excess velocity the shedding angle in the central region, with an assumed uniform approaching velocity, will be reduced to zero, i.e. parallel shedding. Naturally, there will be an overcompensation if the excess velocity is higher than this threshold value. Interestingly, the present results suggested that the shedding can still remain parallel within a substantial central region despite a considerable amount of overcompensation. However, such an overcompensation certainly involves a local increase in the convection velocity and to keep up with a constant shedding frequency the shedding outside this parallel region will become curved (away from the axis towards the ends). As mentioned earlier this shedding behaviour was observed for the case ($Re \approx 100$, $D = 0.5$ mm, $D_{EP}/D = 20$, $L/D = 2000$). The probable influence of aspect ratio on the effect of overcompensation was not investigated. Nevertheless, the measurements strongly suggest that the parallel mode (at $Re > Re_s$) cannot be induced by simply increasing the aspect ratio – at least not with symmetrical circular end plate conditions and for highly uniform upstream conditions.

It is worth noting that Van Atta & Gharib (1987) suggested from their experiments that all discontinuities in the Strouhal–Reynolds number relationship for aspect ratios

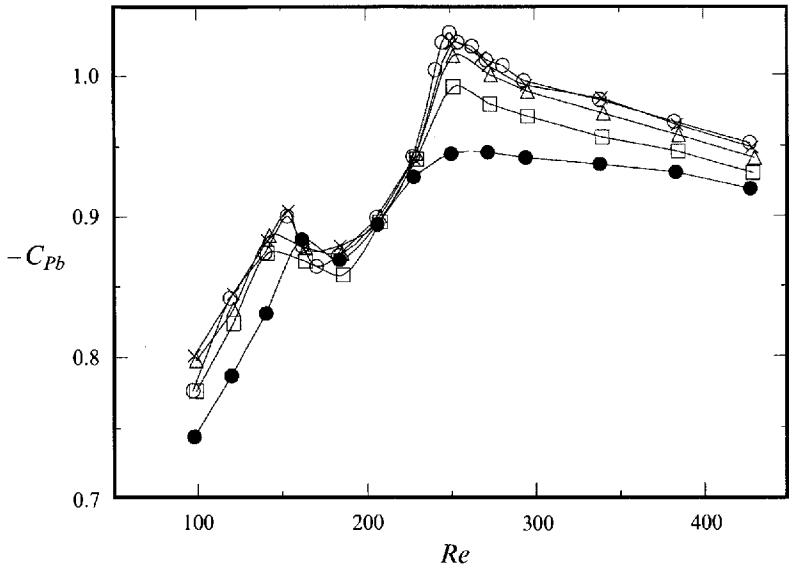

FIGURE 7. Base suction coefficients as measured with the 1 mm cylinder, $D_{EP}/D = 15$, $d/D = 0.20$: ○, $L/D = 480$ (NE); ×, $L/D = 400$; △, $L/D = 200$; □, $L/D = 100$; ●, $L/D = 50$. Lines are drawn for visual aid only.

larger than about 2500 and highly uniform approaching flow can be attributed to flow-induced vibration of the cylinder. This suggestion seems to be in opposition with the present results. However, Van Atta & Gharib used wind tunnel wall-bounded end conditions at these large aspect ratios. As shown by König *et al.* (1990) this type of end condition, with a velocity decrease through relatively thick boundary layers towards the ends, normally introduces another type of shedding mode adjacent to the end cell – the so-called 'X-mode'. The increased number of nodes compared to the end plate case suggests a stronger restraint on the vortex filaments from the ends. However, there will be a successive loss of this restraint when passing over the nodes. Interestingly, König *et al.* (1990) found that an increase in the free-stream turbulence level from about 0.1% to 1% produced parallel shedding in wall-bounded flows ($L/D = 112$) – an effect which they attributed to a greater loss of restraint taken out by the nodes. This cannot, however, explain why the Strouhal number data of Roshko (1954) are so near the parallel shedding data – the free-stream turbulence level in his measurements was about 0.03%. It is worth noting that there is an indication of oblique shedding in Roshko (1954). In his case at ($Re = 80$, $L/D = 322$, $D = 1.58$ mm) a spanwise wavelength of about 18 diameters was observed. With an assumed streamwise wavelength of 5.9 diameters (Williamson 1989) the shedding angle becomes 18°. This is in agreement with the visualizations of wall-bounded flows by König *et al.* (1992) which show an oblique shedding angle of about that magnitude ($Re = 75$–85, $L/D = 336$). However, the bulk of Roshko's laminar shedding data is for much larger aspect ratios (smaller diameters) for which no spanwise correlations were measured. Nevertheless, it seems that we cannot completely eliminate the possibility that certain wall-bounded flows actually will produce parallel shedding at very large aspect ratios.

The present base pressure measurements were only extended down to a Reynolds number of about 100 (see figures 3(*b*) and 7). The base suction coefficient in the laminar shedding regime and for $L/D \geqslant 100$ was seemingly independent of the aspect ratio. The spanwise distributions given by Williamson & Roshko (1990) for $Re = 125$,

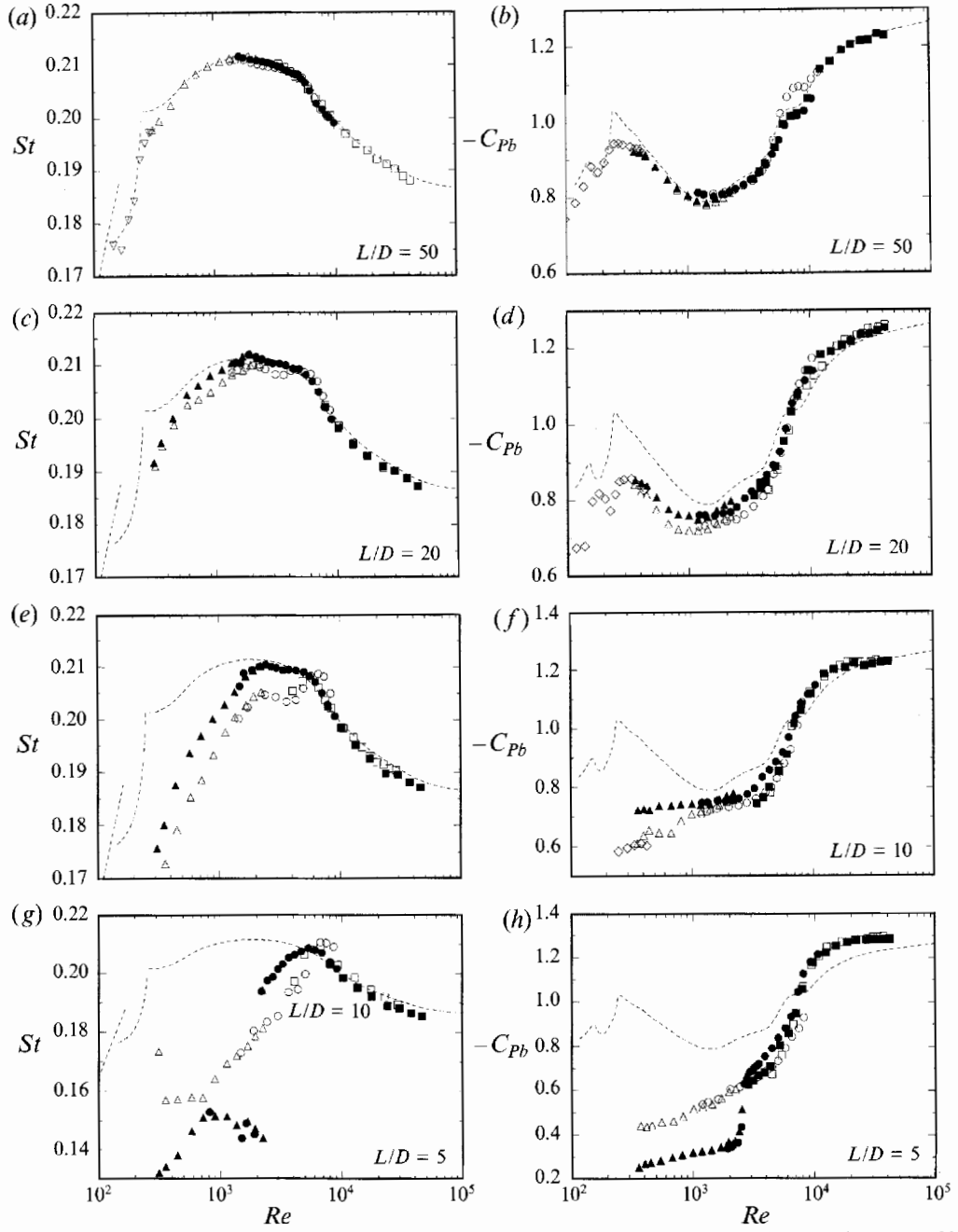

FIGURE 8. Strouhal number and base suction coefficient at different aspect ratios. (*a–b*) $L/D = 50$; (*c–d*) $L/D = 20$; (*e–f*) $L/D = 10$; (*g–h*) $L/D = 5$. Filled symbols, $D_{EP}/D = 10$; open symbols, $D_{EP}/D = 15$. Dotted lines represent smoothed data from figure 2: ▽, $D = 0.5$ mm; (△, ▲), $D = 2$ mm; (○, ●), $D = 6$ mm; (□, ■), $D = 20$ mm. Note the change of the vertical scale.

$L/D = 130$ indicated mid-span values of 0.78 and 0.82 for oblique and parallel shedding, respectively. The interpolated value from figure 7 is 0.83, i.e. about 6% higher compared with the oblique shedding case of Williamson & Roshko. For the largest aspect ratio in figure 7 ($L/D = 480$) and for $Re = 125$, the interpolated base suction coefficient is 0.85. At this aspect ratio the supporting plates acted as end plates

(this end condition is denoted 'NE'). Although not actually verified it can be assumed that the shedding in this case was essentially parallel (owing to the excess free-stream velocity near the ends). Nevertheless, at these low Re, the deviations between the present data and those of Williamson & Roshko (1990) are within the experimental uncertainties.

The present data within the beginning of the transition regime, i.e. from about $Re = 160$ to $Re = 230$, suggested a relatively weak influence of aspect ratio. The flow within this range is highly three-dimensional involving the generation of vortex loops (Williamson 1988*b*) and formation of 'spot-like Λ-structures' associated with vortex dislocations (Williamson 1992). The spanwise scale of the vortex loops appears to be of the order a few diameters (Williamson 1988*b*) while the 'Λ-structures' spread out into spanwise regions as they travel downstream (at half-angles of the order 12°, see Williamson 1992). At these Re the appearance of the dominating broadbanded peak in the measured spectra changed downstream, see also Williamson (1992). This effect probably caused some of scatter in the present Strouhal number data, see figure 4 in which the hot wire was positioned at different streamwise locations ($x/D = 10$–40). Interestingly, the influence of aspect ratio was much stronger at higher Reynolds numbers within the transition regime. At these Re another mode comes into play (Williamson 1988*b*) – in coexistence with the mode found at lower Re (see above). It appears that this new mode is the one which survives the transition at around $Re = 250$ and presumably it involves a much stronger spanwise coupling compared to the other.

As can be judged from some of the previous figures, the most dramatic effects of aspect ratio at low Re occurred for $L/D \leqslant 30$. Changes in the character of the flow at such small aspect ratios and at these low Reynolds numbers are not surprising. In the laminar shedding regime, for instance, the end or wall affected regions, which have a shedding frequency lower than the shedding frequency far from the plates (or the walls), have a size of about 10 diameters. The reader is referred to e.g. Slaouti & Gerrard (1981), Gerich & Eckelmann (1982), Williamson (1989), König *et al.* (1990), Williamson & Roshko (1990) and Lee & Budwig (1991) for a discussion of further aspect ratio effects at these low L/D as well as effects of different end configurations.

3.3. *Reynolds numbers higher than about* 250

Figure 8 shows the Reynolds number effects on the Strouhal number and the base suction coefficient at aspect ratios $L/D = 5$, 10, 20 and 50, respectively ($D_{EP}/D = 10$ and 15). The influence of aspect ratio at $D_{EP}/D = 10$ and 15 on the base suction coefficient, as measured with the 6 mm cylinder, are depicted in figure 9. Starting with figures 8(*a*) and 8(*b*), at $L/D = 50$, the largest deviations from the 'quasi-infinite cylinder' appeared for Reynolds numbers lower than, say, $Re = 600$. The maximum deviation occurred at $Re \approx 250$, i.e. around the 'second transition' towards turbulence (Williamson 1988*b*). In fact, to avoid any influence of aspect ratio at mid-span, within the experimental uncertainties, L/D of the order of 200 were needed at and around this transition (see also figure 7), whereas L/D of the order of 100 was required up to $Re \approx 600$. An aspect ratio of 50 was, however, sufficient between $Re \approx 600$ and $Re \approx 4000$ and also for $Re > 10^4$.

At the aspect ratio of 50, the interesting feature of a plateau in the base suction coefficient at $Re \approx 6 \times 10^3$–8×10^3 was captured (the plateau was not facility-dependent; it was present also in the flow visualization wind tunnel). There was however a discrepancy between the two relative end-plate diameters (10 and 15) (see figure 8*b*). As seen in figure 9, an aspect ratio higher than about 70 was needed for independent conditions with the larger end-plate diameter whereas $L/D \approx 60$ was

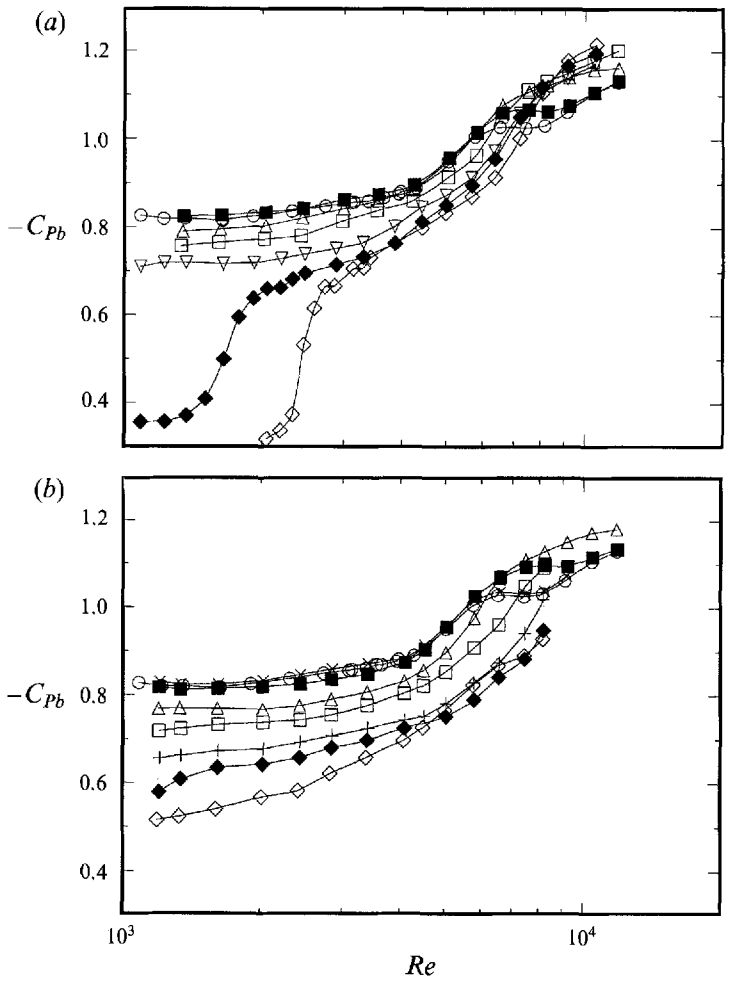

FIGURE 9. Base suction coefficients *vs.* Reynolds number at different aspect ratios as measured with the 6 mm cylinder. (*a*) $D_{EP}/D = 10$, (*b*) $D_{EP}/D = 15$: ○, $L/D = 80$ (NE); ×, 70; ■, 50; △, 30; □, 15; ▽, 7.5; +, 7; ◆, 6; ◇, 4. Lines are drawn for visual aid only.

sufficient for $D_{EP}/D = 10$. Possibly, the reason that the effect shows up at these relatively large aspect ratios is the surprisingly large axial correlation associated with the transitional changes at around $Re = 5 \times 10^3$ (Norberg 1987, 1989). At Reynolds numbers below the transition the pressure in the base region of the cylinder is more or less constant whereas there is an increase in suction towards the base ($\phi = 180°$) at higher Re (see e.g. Norberg 1987). However, this redistribution of base pressures and its relation to the existence of the plateau need further elucidation.

An interesting detail was that the curves with Strouhal number *vs.* Re, all passed through a value of $St = 0.21$ at around $Re = 5.5 \times 10^3$, for any aspect ratio. Nevertheless, the measurements taken as a whole indicated that aspect ratios of the order 60–70 were needed in the range $Re = 4 \times 10^3$–10^4. Gowda (1975) found negligible effects on St for aspect ratios higher than about $L/D = 45$ ($D_{EP}/D = 10$, $Re = 10^3$–10^4), in general agreement with the present results.

At aspect ratios smaller than about $L/D = 30$ the relative end plate diameter was a much more important parameter, at least up to $Re \approx 5 \times 10^3$, see e.g. figures 8(*c–h*) and 9. As shown by Kubo *et al.* (1989), for $L/D = 20$, an increase in the relative end-plate

diameter from $D_{EP}/D = 4$ to 10 resulted in a 20% increase in the base suction coefficient ($Re = 5 \times 10^3$–4×10^4); a further increase up to $D_{EP}/D = 16$ only gave an increase of some per cent, in agreement with present results (see figure 8*d*). At $L/D = 20$ and $L/D = 10$ and for $Re < 5 \times 10^3$, however, the larger end-plate diameter gave both significantly lower Strouhal number and lower base suction coefficient in comparison with values obtained with the smaller end-plate diameter (see figure 8*c–f*). That an increase in the relative end-plate diameter results in a larger end effect is in accordance with Stäger & Eckelmann (1991) who found that for a given Reynolds number ($Re = 300$–5000) the affected region near to an end plate decreases with decreasing relative end plate diameter. A reversed situation between the two relative end plate diameters was observed at smaller aspect ratios and for even lower Re, see figures 8(*g–h*) and 9. According to Stäger & Eckelmann (1991) the affected region near to an end plate, at these Re and D_{EP}/D, is of the order of five diameters. It therefore seems very plausible that dramatic changes will occur when the aspect ratio becomes smaller than $L/D \approx 10$. Indeed, for $D_{EP}/D = 10$, at L/D smaller than about 7 and for Re lower than about 3×10^3 a bi-stable flow was observed. Some details about this phenomenon are given in the following section.

3.4. *Bi-stable flow*

It was noticed by Gerich (1986) that the vortex shedding periodicity, at intermediate Reynolds numbers, i.e. at around $Re = 2 \times 10^3$, disappeared at aspect ratios lower than some critical value. The critical aspect ratios decreased from about 7 at $Re = 1360$ to about 4 at $Re = 2600$. The relative end-plate diameter in those experiments was 10 (which is the same value for which the appearance of the bi-stable flow was found in the present case). Gerich also noticed, in some of his cases, that the hot-wire signal displayed unsteady transitions between different amplitude levels. Although not clearly stated in the report, it is obvious that the flow in these cases was bi-stable, i.e. the flow switched between two modes. In addition, he noticed that the phenomenon was not dependent on the background disturbances in the wind tunnel. Interestingly, Relf (1914) mentions an 'unstable region' at around these Reynolds numbers ($Re = 10^3$ to 3×10^3). He observed in his delicate measurements of drag on wires 'two definite balance points... the balance changing over from one to the other at short intervals'. This seemingly bi-stable condition was attributed to 'the instability of flow' (aspect ratio was not stated).

In the present case, simultaneous variations in near-wake velocity as well as in the base pressure were monitored. It was then fully realized that the flow, at some aspect ratios and in rather narrow ranges of the Reynolds number, was bi-stable. With the larger relative end plates, however, i.e. for $D_{EP}/D = 15$, the flow remained in the regular shedding mode for all aspect ratios which were investigated ($L/D \geqslant 2$). It should be noted that the bi-stable flow was also observed with the 2 mm cylinder but in this case it was not possible to follow the fast switches in the base pressure. The transition between the two modes did not seem to possess hysteresis effects.

Why then, did only the smaller end-plate diameter show this behaviour and why only in this narrow range of intermediate Reynolds numbers? The explanation is probably related to the observed variation of the vortex formation length. At large aspect ratios, the formation length has a local maximum of about 3 diameters at around $Re = 1.5 \times 10^3$. This means that the first roll-up of the primary vortex in the regular shedding process takes place on average at around 3 diameters downstream of the cylinder axis. With a relative end-plate diameter of 10 the edge of the plate is five diameters behind the cylinder, i.e. only two diameters away from the mean roll-up

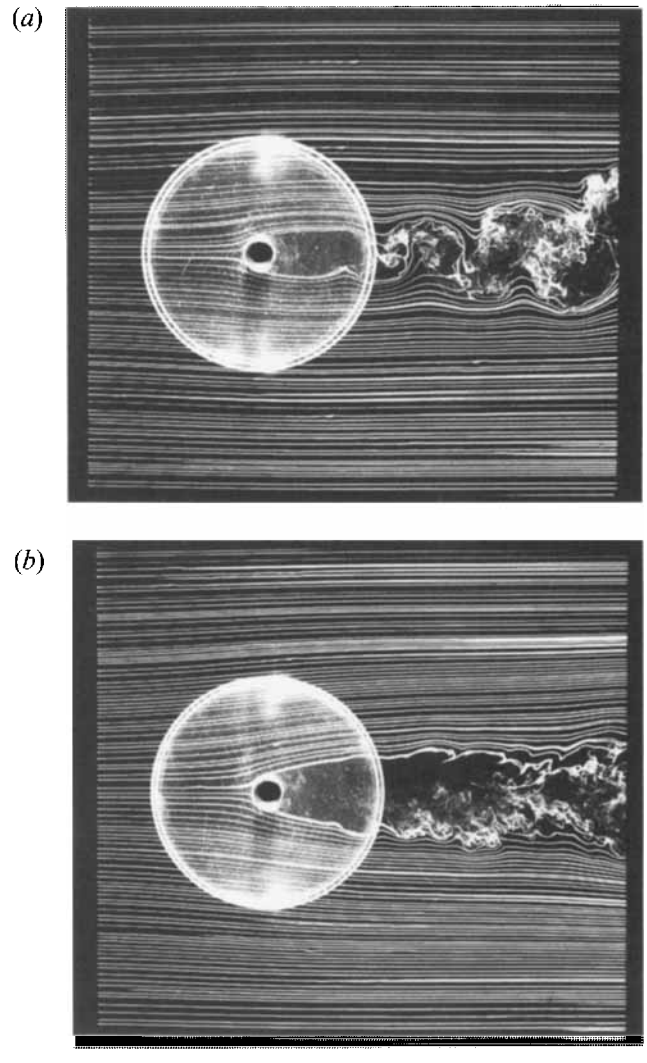

FIGURE 10. Smoke-wire visualizations of bi-stable flow ($Re = 2 \times 10^3$, $D = 10$ mm, $L/D = 5$, $D_{EP}/D = 10$), (*a*) vortex shedding (mode *A*), (*b*) irregular flow (mode *B*).

position. In addition, flow visualizations at these Reynolds numbers showed that the vortex formation length increased with decreasing aspect ratio. Thus, it seems very likely that the first appearance of the irregular mode at these Re is a consequence of the vortex roll-up occasionally occurring close to the downstream edge of the end plate. As the vortex formation region is associated with a low pressure an axial flow may arise around the edge from the outside. This possible inflow may eventually destroy the development of the vortex shedding with the result of an increase of the pressure in the base region. With the flow in this mode, and at appropriate Reynolds number, the wake flow might develop natural disturbances in the shear layers which can initiate a change to the vortex shedding mode again, i.e. bi-stable flow. Obviously, the scenario is dependent on the downstream extent of the end plate. With a large relative end-plate diameter, the vortex formation region is effectively shielded from the outside flow.

While the distance to downstream edge seems to be responsible for the dramatic changes at small aspect ratios at these intermediate Reynolds numbers it seems that the

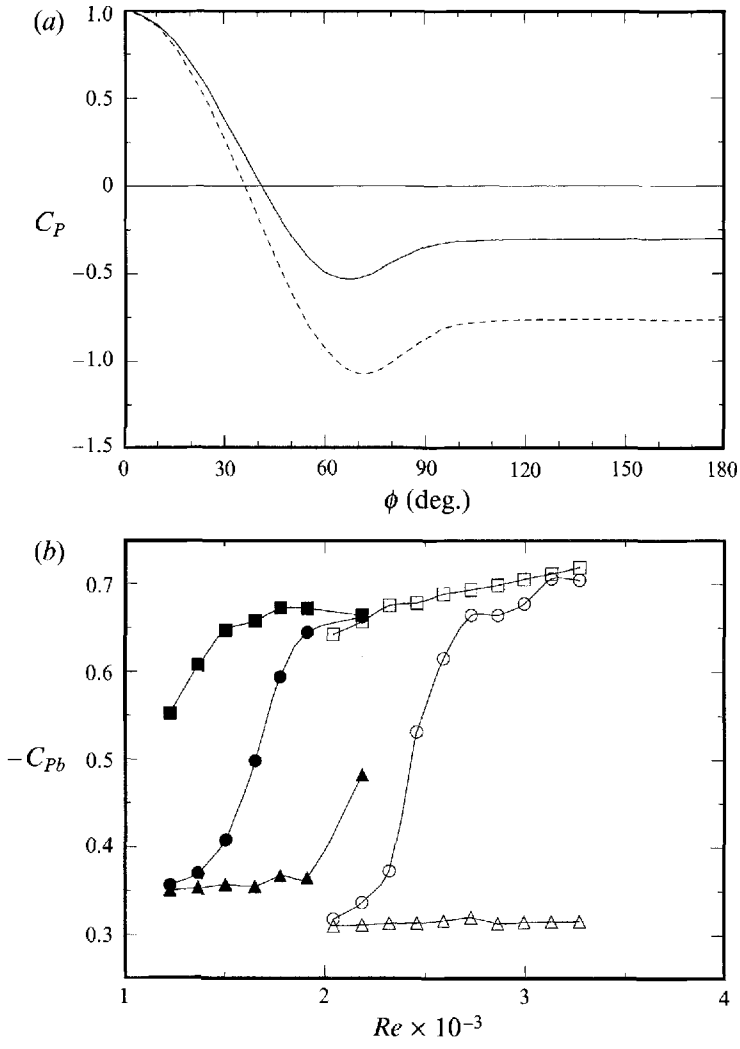

FIGURE 11. (*a*) Pressure distributions at $Re = 1.5 \times 10^3$: ——, $(L/D, C_{DP}) = (5, 0.61)$; – – –, $(50, 0.89)$. C_{DP}, pressure drag coefficient. The angles have been corrected owing to the finite pressure hole size, as outlined by Linke (1931). (*b*) Base suction coefficients in the range where the flow was bi-stable: open markers, $L/D = 4$; solid markers, $L/D = 6$; □, Strouhal mode (*A*); △, irregular mode (*B*); ○, total $(A+B)$. $D = 6$ mm, $D_{EP}/D = 10$.

distance to the upstream edge becomes more important at higher Reynolds numbers. In the investigation by Szepessy (1993) it was found, by keeping an aspect ratio of about unity in combination with using a short leading-edge distance (rectangular end plates), that the vortex shedding became inhibited, probably resulting in a very steady wake for $Re < 1.1 \times 10^4$. He also noticed that the transition between the two modes was hysteretic and not bi-stable as a single disturbance would trigger the onset of regular vortex shedding, whereas the steady wake could only be obtained with slowly accelerating the flow from zero velocity.

Smoke-wire visualizations showed that the flow in the mode with the lowest base suction was highly irregular with no alternating vortex shedding, see figure 10(*b*). The quiescent near-wake flow in the irregular mode indicated a steady laminar separation. At some distance downstream the wake became turbulent.

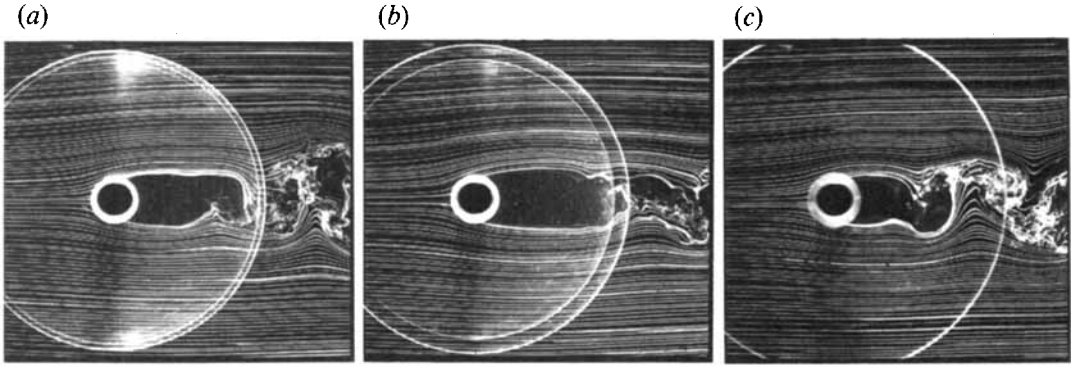

FIGURE 12. Smoke-wire visualizations for (*a*) $L/D = 2$, (*b*) $L/D = 5$ and (*c*) $L/D = 15$ ($Re = 3 \times 10^3$, $D = 20$ mm, $D_{EP}/D = 10$).

Typical pressure distributions for the different modes are shown in figure 11(*a*) ($Re = 1.5 \times 10^3$). In the pressure distribution for $L/D = 5$, i.e. (stable) irregular flow, the surface pressure was equal to the free-stream static pressure at around $\phi = 41°$ while the highest suction occurred at around $\phi = 68°$. The corresponding angles for $L/D = 50$, i.e. (stable) vortex shedding flow, was 36° and 71°, respectively. In both cases a laminar separation at $\phi = 80°$–$84°$ was indicated. The pressure distribution for $L/D = 5$ as well as the general appearance of the flow in the irregular mode, as judged from smoke-wire visualizations, compare very well with the above-mentioned 'inhibited vortex shedding flow' as reported by Szepessy (1993). As seen in the snapshot of the flow in the vortex shedding mode in figure 10(*a*), the vortex formation occurred close to the downstream edge of the end plate.

Detailed variations of the base suction coefficient with Re, in the bi-stable flow ranges, are shown in figure 11(*b*). The mode corresponding to regular vortex shedding is denoted by capital letter A ('Strouhal mode') whereas the mode without strong periodicity is denoted by B ('irregular mode'). $A + B$ represents the observed long-time mean flow condition. The values for the individual modes were taken from the peaks in the measured probability density functions, see figure 13(*a*). The disappearance of vortex shedding periodicity was only observed for L/D lower than 7, see figure 9(*a*). With an aspect ratio of 6 the switch between the modes started at $Re \approx 1200$ and ended at $Re \approx 2200$. The corresponding ranges for $L/D = 5$ and 4 were $Re \approx 1800$–3200 and $Re \approx 2000$–3400, respectively. At even smaller aspect ratios the bi-stable Reynolds number range became more narrow. For $L/D = 2$ the range extended from about $Re \approx 2700$ to $Re \approx 2900$. As shown in figure 12, for $Re \approx 3000$, the regular vortex shedding found at $L/D = 15$ was seen to occur also for $L/D = 2$ whereas the intermediate $L/D = 5$ caused suppression of the vortex shedding (bi-stable).

In the irregular mode the already very low base suction showed a further decrease with decreasing aspect ratio. For an aspect ratio of $L/D = 5$, the flow remained in the irregular mode down to at least $Re = 350$ where the base suction coefficient was as low as 0.25, see figure 8(*h*). The irregular flow condition did exhibit some degree of periodicity. The dominating peaks were, however, broadbanded with relative bandwidths (−3 dB) of the order 10%. The Strouhal numbers for $L/D = 5$ showed an increase with increasing Re from $St \approx 0.13$ at $Re \approx 300$ up to $St \approx 0.15$ at $Re \approx 750$ (figure 8*g*). A slight declining trend was indicated at higher Re.

The measured spectra in the irregular mode showed that the near-wake velocity fluctuations contained relatively more energy at high frequencies than within the

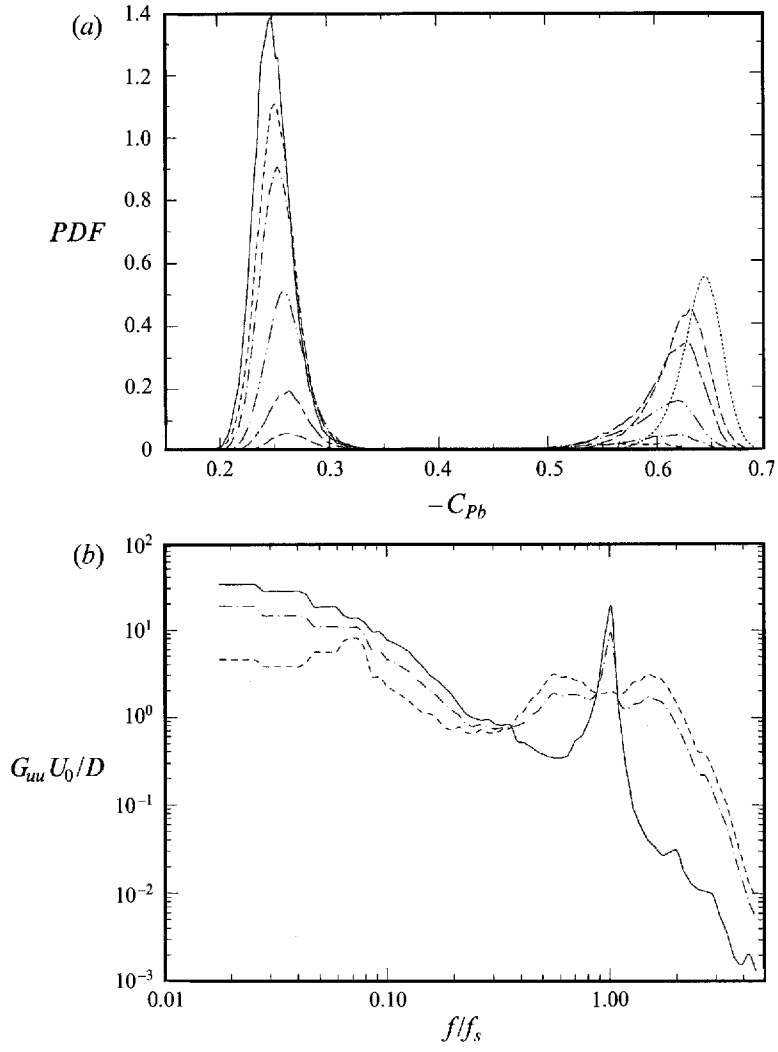

FIGURE 13. Bi-stable flow (D = 6 mm, L/D = 5, D_{EP}/D = 10). (*a*) Probability density functions (PDF) of the base suction coefficient: ——, ($Re \times 10^{-3}$, I[%]) = (2.04, 1); – – –, (2.22, 5); —·—, (2.39, 10); —··—, (2.69, 33); ———, (2.84, 72); ———, (3.00, 90); ···, (3.16, 99). I, Intermittency factor, i.e. fraction of time spent in the Strouhal mode. (*b*) Normalized power spectral density of velocity fluctuations in the near-wake at $Re = 2.7 \times 10^3$ (x/D = 5): ——, Strouhal mode (A); – – –, irregular mode (B); —·—, total ($A+B$). St = 0.199.

Strouhal mode. The case shown in figure 13(*b*) corresponds to a Reynolds number where the intermittency factor was of the order 50%, i.e. approximately equal time spent in both modes. Within the bi-stable flow the narrow-banded peak corresponding to the Strouhal mode was surrounded by two broadbanded peaks from the irregular mode (see figure 13*b*). The velocity fluctuations in the irregular mode did not contain as much energy at low frequencies as in the Strouhal mode. The broadbanded peak at around $f/f_S \approx 0.07$ ($St = 0.015$) was only present within the bi-stable flow range. At lower Reynolds numbers, the traces of regular anti-symmetrical shedding gradually disappeared while the leftmost peak of the irregular mode, as seen in figure 13(*b*), became the most dominating one. Also, a peak at around $St = 0.4$ became discernible at the lower end of the bi-stable range. This is an indication of symmetrical vortex

shedding. Elements of symmetrical vortex shedding within the irregular mode were in fact seen in the flow visualizations.

4. Conclusions and final remarks

4.1. *Laminar shedding flow*

Within the laminar shedding type of flow the particular concern was to investigate 'large' aspect ratios, i.e. L/D higher than about 100 and up to several thousand. The findings at aspect ratios lower than about $L/D = 100$ were in general agreement with Williamson (1989) and König *et al.* (1990).

The critical Reynolds number for onset of vortex shedding (Re_c) was practically constant at aspect ratios larger than about 40 ($Re_c \approx 47.4$). At smaller aspect ratios, however, the onset was delayed ($L/D = 20 \Rightarrow Re_c \approx 51.5$).

At aspect ratios larger than about 100 and for highly uniform upstream conditions, the measured Strouhal numbers (at around mid-span) were independent of the aspect ratio. In such cases, however, an essentially parallel shedding condition was only indicated at Reynolds numbers lower than about 70. At around this Reynolds number (Re_s) there was a transitional change between a parallel mode found at $Re < Re_s$ and an oblique mode. The transition produced a discontinuity in the Strouhal–Reynolds number relationship. The measurements strongly suggested that the parallel mode cannot be induced above Re_s by simply increasing the aspect ratio – at least not with symmetrical circular end plate conditions and for highly upstream conditions (aspect ratios up to several thousand were investigated).

However, parallel (or very near parallel) shedding was observed throughout the laminar shedding regime in some (high-aspect-ratio) cases when there was a slight but symmetrical increase in the approaching free-stream velocity towards the movable end plates (the velocity increase was caused by the supporting plates which were placed vertically within the wind tunnel). This is in support of the working principle in producing parallel shedding as stated by Albarède & Monkewitz (1992), i.e. an increase in free-stream velocity towards the cylinder ends (as shown by e.g. Williamson & Roshko (1990) and Eisenlohr (1990), there is an incrcase in base suction towards the ends in parallel shedding flow). When the end plates were placed where the approaching velocity was about 7.5% above the value far from the end plates, and for $Re \approx 100$, an essentially parallel shedding condition was indicated within a substantial central region of the span (shedding angle within $\pm 1°$, $z/D \approx \pm 100$). Outside this region there was a gradual increase in the shedding angle away from the cylinder axis towards the ends (approximately 6° at 200 diameters from mid-span) thus suggesting an overstimulation from the conditions at the ends. It should be noted, however, that the essentially parallel condition in this case was only present over about 10% of the total span. Interestingly, at this Re, it was indicated that the necessary excess in the free-stream velocity to produce parallel shedding was of the order 2% – in agreement with the threshold value as indicated by Miller & Williamson (1993) in conjunction with the method of 'end suction'. Presumably, with this 'optimum' excess velocity at the ends the shedding would be parallel over a much larger part of the span.

The base pressure measurements were only extended down to $Re \approx 100$. At $L/D > 50$ the variations with aspect ratio were negligible (within the experimental uncertainties). At smaller L/D a decrease in base suction with decreasing L/D was indicated. At Reynolds numbers higher than about 150 and for large aspect ratios the flow was occasionally disrupted by a change to three-dimensional flow (presumably caused by intrinsic instabilities) and beyond $Re \approx 168$ no regular laminar shedding

could be established. The Strouhal–Reynolds number relationship for the laminar parallel shedding flow was in excellent agreement with the relation given by Williamson (1988*a*).

4.2. *Transitional and turbulent flow*

In transitional and turbulent flow around a nominally two-dimensional circular cylinder, the spanwise radius of action associated with the naturally evolving (intrinsic) three-dimensional flow structures might be considered to be limited. Likewise, in real experiments with finite cylinders, the extrinsic influences of the specific end conditions may also be considered as limited. We therefore expect the flow at around mid-span to be effectively decoupled from the end effects at some finite aspect ratio. Naturally, the required aspect ratio stated for this 'quasi-infinite' cylinder will, to a certain degree, be a reflection on the experimental uncertainties.

In the beginning of the transition regime, i.e. from $Re \approx 160$ to 230, aspect ratios of the order 50 were needed in order to represent the flow around a 'quasi-infinite' cylinder. At around the transition occurring at $Re \approx 250$, however, an aspect ratio larger than about 200 was indicated. At higher Reynolds numbers, the corresponding aspect ratios required for independent conditions at mid-span, within the experimental uncertainties, were as follows: $350 < Re < 600$: $L/D \geqslant 100$, $600 \leqslant Re < 4000$: $L/D \geqslant 50$, $4000 \leqslant Re < 10^4$: $L/D \geqslant 60$–70 and finally $10^4 \leqslant Re < 4 \times 10^4$: $L/D \geqslant 25$. It should be pointed out that these limits, which are supposed to be conservative, may be reduced when using more optimized end-plate designs. Nevertheless, as the regions which are directly affected by the end conditions ('end cells') remain smaller than about 5 diameters and show a decrease with increasing Reynolds number (Stäger & Eckelmann 1991), it can be suspected that the required aspect ratio for reaching independent conditions is more or less linearly related to the 'undisturbed' axial correlation length. Unfortunately, experimental data on axial correlation are rather limited, at least for $Re < 10^3$. The data at $Re \leqslant 10^3$, however, with a one-sided axial correlation length of about 10 diameters at $Re = 10^3$, 15 diameters at around $Re = 5000$, five diameters at around $Re = 10^4$ decreasing to about three diameters at the upper end of the subcritical regime at $Re \approx 2 \times 10^5$ (Bruun & Davies 1975; Norberg 1989), indicate that aspect ratios larger than four to five times this length are required for reaching this independent state. More measurements are needed in order to verify this approximate linear relationship at even lower Reynolds numbers. In particular, the three-dimensionalities and spanwise scales associated with the generation of Strouhal vortices and shear-layer streamwise vortices as well as their interactions need further elucidation.

In the approximate range $350 < Re < 4000$ and roughly for $10 < L/D < 30$, an increase in the relative end-plate diameter, from $D_{EP}/D = 10$ to $D_{EP}/D = 15$, resulted in the decrease in both Strouhal number and base suction. At Re higher than about 10^4, however, this change of end-plate diameter only resulted in very small changes in these quantities.

With the smallest relative end plate diameter only ($D_{EP}/D = 10$) and for aspect ratios smaller than 7, a bi-stable flow showing switches between regular vortex shedding and 'irregular flow' was found at intermediate Reynolds number ranges in the subcritical regime ($Re \approx 2 \times 10^3$). It is suggested that the appearance of this phenomenon is related to the observed variations in the vortex formation length that may be caused by axial flow disturbances imposed at the downstream edge of the end plate.

It has been a great pleasure to communicate at length with Charles Williamson –

especially about basc pressure measurements at low Reynolds numbers. The author also wishes to thank his colleague Lars Davidson for the supply of results from numerical simulations around the supporting plates. Finally, the support from the Swedish Research Council for Engineering Sciences (TFR) during the final stages of this investigation is gratefully acknowledged.

REFERENCES

ALBARÈDE, P. & MONKEWITZ, P. A. 1992 A model for the formation of oblique shedding and 'chevron' patterns in cylinder wakes. *Phys. Fluids* A **4**, 744–756.

BATCHO, P. & KARNIADAKIS, G. E. 1991 Chaotic transport in two- and three-dimensional flow past a cylinder. *Phys. Fluids* A **3**, 1051–1062.

BEARMAN, P. W. 1969 On vortex shedding from a circular cylinder in the critical Reynolds number regime. *J. Fluid Mech.* **37**, 577–585.

BLEVINS, R. D. 1985 The effect of sound on vortex shedding from cylinders. *J. Fluid Mech.* **161**, 217–237.

BLOOR, S. 1964 The transition to turbulence in the wake of a circular cylinder. *J. Fluid Mech.* **19**, 290–304.

BRUUN, H. H. & DAVIES, P. O. A. L. 1975 An experimental investigation of the unsteady pressure forces on a circular cylinder in a turbulent cross flow. *J. Sound Vib.* **40**, 535–559.

COWDREY, C. F. 1963 A note on the use of end plates to prevent three-dimensional flow at the ends of bluff cylinders. *ARC Current Papers* 683.

DENNIS, S. C. R. & CHANG, G.-Z. 1970 Numerical solutions for steady flow past a circular cylinder at Reynolds numbers up to 100. *J. Fluid Mech.* **42**, 471–489.

EISENLOHR, H. 1990 Ein kurzer oder ein langer Zylinder: Worin liegt der Unterschied für die Kármánsche Wirbelstraße? *Mitt. Max-Planck-Institut für Strömungsforschung, Göttingen* 98.

EISENLOHR, H. & ECKELMANN, H. 1989 Vortex splitting and its consequences in the vortex street wake of cylinders at low Reynolds numbers. *Phys. Fluids* A **1**, 189–192.

FAGE, A. 1913 Determination of the pressure distribution round a cylinder. *Adv. Commun. Aero. R&M* 106.

FOX, T. A. & WEST, G. S. 1990 On the use of end plates with circular cylinders. *Exps Fluids* **9**, 237–239.

GERICH, D. 1986 Über die Veränderung der Kármánschen Wirbelstraße durch Endscheiben an einem Kreiszylinder. *Mitt. Max-Planck-Institut für Strömungsforschung, Göttingen* 81.

GERICH, D. & ECKELMANN, H. 1982 Influence of end plates and free ends on the shedding frequency of circular cylinders. *J. Fluid Mech.* **122**, 109–121.

GERRARD, J. H. 1965 A disturbance-sensitive Reynolds number range of the flow past a circular cylinder. *J. Fluid Mech.* **22**, 187–196.

GOWDA, B. H. L. 1975 Some measurements on the phenomenon of vortex shedding and induced vibrations of circular cylinders. *Deutsche Luft- und Raumfahrt, Forschungsbericht* 75-01.

GRAHAM, J. M. R. 1993 Report on the session comparing computation of flow past circular cylinders with experimental data. In *Proc. IUTAM Symp. Bluff-Body Wakes, Dynamics and Instabilities, 7–11 September 1992, Göttingen*, pp. 317–323. Springer.

HAMMACHE, M. & GHARIB, M. 1989 A novel method to promote parallel vortex shedding in the wake of circular cylinders. *Phys. Fluids* A **1**, 1611–1614.

HAMMACHE, M. & GHARIB, M. 1991 An experimental study of the parallel and oblique vortex shedding from circular cylinders. *J. Fluid Mech.* **232**, 567–590.

HOMANN, F. 1936 Der Einfluss grösser Zähigkeit bei der Strömung um den Zylinder und um die Kugel. *Z. angew. Math. Mech.* **6**, 153–164.

KATO, C. & IKEGAWA, M. 1991 Large eddy simulation of unsteady turbulent wake of a circular cylinder using the finite element method. *Advances in Numerical Simulation of Turbulent Flows ASME 1991*, FED 117, pp. 49–56.

KEEFE, R. T. 1961 An investigation of the fluctuating forces acting on a stationary circular cylinder in a subsonic stream, and of the associated sound field. *UTIA Rep.* 76.

KUBO, Y., MIYAZAKI, M. & KATO, K. 1989 Effects of end plates and blockage of structural members on drag forces. *J. Wind Engng Indust. Aero.* **32**, 329–342.

KÖNIG, M., EISENLOHR, H. & ECKELMANN, H. 1990 The fine structure in the Strouhal–Reynolds number relationship of the laminar wake of a circular cylinder. *Phys. Fluids* A **2**, 1607–1614.

KÖNIG, M., EISENLOHR, H. & ECKELMANN, H. 1992 Visualization of the spanwise cellular structure of the laminar wake of wall-bounded circular cylinders. *Phys. Fluids* A **4**, 869–872.

LEE, T. & BUDWIG, R. 1991 A study of the effect of aspect ratio on vortex shedding behind circular cylinders. *Phys. Fluids* A **3**, 309–315.

LINKE, W. 1931 Neue Messungen zur Aerodynamik des Zylinders, insbesondere seines reinen Reibungswiderstandes. *Z. Phys.* **22**, 900–914.

MATHIS, C., PROVANSAL, M. & BOYER, L. 1984 The Bénard–von Kármán instability: an experimental study near the threshold. *J. Phys. Lett. Paris* **45**, 483–491.

MILLER, G. D. & WILLIAMSON, C. H. K. 1993 The control of transient and steady-state three-dimensional shedding patterns using variable suction end boundary conditions. *Exps. Fluids* (submitted).

NISHIOKA, M. & SATO, H. 1974 Measurements of velocity distributions in the wake of a circular cylinder at low Reynolds numbers. *J. Fluid Mech.* **65**, 97–112.

NORBERG, C. 1987 Effects of Reynolds number and a low-intensity freestream turbulence intensity on the flow around a circular cylinder. Publ. 87/2 Dept. Applied Thermodynamics and Fluid Mechanics, Chalmers University of Technology.

NORBERG, C. 1989 An experimental study of the circular cylinder in cross flow: transition around $Re = 5 \cdot 10^3$. In *Proc. 4th Asian Congress of Fluid Mechanics, Suppl. Vol.* pp. C240–C243. University of Hong Kong.

NORBERG, C. 1993 Pressure forces on a circular cylinder in cross flow. In *Proc. IUTAM Symp. Bluff-Body Wakes, Dynamics and Instabilities, 7–11 September 1992, Göttingen*, pp. 275–278. Springer.

RELF, E. F. 1914 Discussion of results of measurements of the resistance of wires, with some additional tests on the resistance of wires of small diameter. *Adv. Commun. Aero. R & M* 102.

ROSHKO, A. 1954 On the development of turbulent wakes from vortex streets. *NACA Rep.* 1191.

ROSHKO, A. & FISZDON, W. 1969 On the persistence of transition in the near-wake. In *Problems of Hydrodynamics and Continuum Mechanics*, pp. 606–619. Society of Industrial and Applied Mathematics, Philadelphia.

SLAOUTI, A. & GERRARD, J. H. 1981 An experimental investigation of the end effects on the wake of a circular cylinder. *J. Fluid Mech.* **112**, 297–314.

STANSBY, P. K. 1974 The effects of end plates on the base pressure coefficient of a circular cylinder. *Aero. J.* **78**, 36–37.

STÄGER, R. & ECKELMANN, H. 1991 The effect of endplates on the shedding frequency of circular cylinders in the irregular range. *Phys. Fluids* A **3**, 2116–2121.

SZEPESSY, S. 1993 On the control of circular cylinder flow by end plates. *Euro. J. Mech. B/Fluids* **12**, 217–244.

SZEPESSY, S. & BEARMAN, P. W. 1992 Aspect ratio and end plate effects on vortex shedding from a circular cylinder. *J. Fluid Mech.* **234**, 191–217.

TAMURA, T., OHTA, I. & KUWAHARA, K. 1990 On the reliability of two-dimensional simulation for unsteady flows around a cylinder-type structure. *J. Wind Engng Indust. Aero.* **35**, 275–298.

THOM, A. 1928 An investigation of fluid flow in two dimensions. *Aero Res. Commun. R & M* 1194.

VAN ATTA, C. W. & GHARIB, M. 1987 Ordered and chaotic vortex streets behind circular cylinders at low Reynolds numbers. *J. Fluid Mech.* **174**, 113–133.

WEST, G. S. & APELT, C. J. 1982 The effects of tunnel blockage and aspect ratio on the mean flow past a circular cylinder with Reynolds numbers between 10^4 and 10^5. *J. Fluid Mech.* **114**, 361–377.

WIESELSBERGER, C. 1922 Weitere Feststellungen über die Gesetze des Flüssigkeitsund Luftwiderstandes. *Z. Phys.* **23**, 219–224.

WILLIAMSON, C. H. K. 1988*a* Defining a universal and continuous Strouhal–Reynolds number relationship for the laminar vortex shedding of a circular cylinder. *Phys. Fluids* **31**, 2742–2744.

WILLIAMSON, C. H. K. 1988*b* The existence of two stages in the transition to three-dimensionality of a cylinder wake. *Phys. Fluids* **31**, 3165–3168.

WILLIAMSON, C. H. K. 1989 Oblique and parallel modes of vortex shedding in the wake of a circular cylinder at low Reynolds numbers. *J. Fluid Mech.* **206**, 579–627.

WILLIAMSON, C. H. K. 1992 The natural and forced formation of spot-like 'vortex dislocations' in the transition of a wake. *J. Fluid Mech.* **243**, 393–441.

WILLIAMSON, C. H. K. 1993 Three-dimensional phenomena in bluff body wakes: Part 1: 3-D phase dynamics, Part 2: wave interactions in the far wake. In *Proc. IUTAM Symp. Bluff-Body Wakes, Dynamics and Instabilities, 7–11 September 1992, Göttingen*, pp. 333–336. Springer.

WILLIAMSON, C. H. K. & ROSHKO, A. 1990 Measurements of base pressure in the wake of a cylinder at low Reynolds numbers. *Z. Flugwiss. Weltraumforschung* **14**, 38–46.